*Review*

# Fluorescence Microscopy—An Outline of Hardware, Biological Handling, and Fluorophore Considerations

Shane M. Hickey *[ID], Ben Ung *[ID], Christie Bader, Robert Brooks, Joanna Lazniewska [ID], Ian R. D. Johnson [ID], Alexandra Sorvina [ID], Jessica Logan, Carmela Martini, Courtney R. Moore [ID], Litsa Karageorgos, Martin J. Sweetman [ID] and Douglas A. Brooks [ID]

Clinical and Health Sciences, University of South Australia, Adelaide 5000, Australia; christie.bader@unisa.edu.au (C.B.); robert.brooks@unisa.edu.au (R.B.); joanna.lazniewska@unisa.edu.au (J.L.); ian.johnson@unisa.edu.au (I.R.D.J.); alexandra.sorvina@unisa.edu.au (A.S.); jessica.logan@unisa.edu.au (J.L.); carmela.martino@unisa.edu.au (C.M.); courtney.moore@unisa.edu.au (C.R.M.); litsa.karageorgos@unisa.edu.au (L.K.); martin.sweetman@unisa.edu.au (M.J.S.); doug.brooks@unisa.edu.au (D.A.B.)
* Correspondence: shane.hickey@unisa.edu.au (S.M.H.); ben.ung@unisa.edu.au (B.U.)

**Abstract:** Fluorescence microscopy has become a critical tool for researchers to understand biological processes at the cellular level. Micrographs from fixed and live-cell imaging procedures feature in a plethora of scientific articles for the field of cell biology, but the complexities of fluorescence microscopy as an imaging tool can sometimes be overlooked or misunderstood. This review seeks to cover the three fundamental considerations when designing fluorescence microscopy experiments: (1) hardware availability; (2) amenability of biological models to fluorescence microscopy; and (3) suitability of imaging agents for intended applications. This review will help equip the reader to make judicious decisions when designing fluorescence microscopy experiments that deliver high-resolution and informative images for cell biology.

**Keywords:** fluorescence microscopy; microscopy techniques; imaging agents; cellular imaging

## 1. Introduction

Since the inception of fluorescence microscopes in the early 1900s, their use as a research tool for observing discrete subcellular structures and processes has grown immensely [1]. Initially, auto-fluorescent specimens were visualised with fledgling fluorescence microscopes, until the introduction of fluorescent stains in the 1930s, which enabled non-fluorescent specimens to be visualised [2]. The use of fluorescently-labelled antibodies in the 1940s [3] enabled precision visualisation of target structures in cells, and with the Nobel prize winning discovery of green fluorescent proteins (GFP) in the 1960s and their subsequent development as a genetic tag [4], the field has evolved to permit targeted live cell imaging. The discovery of novel fluorescent markers has driven the development of fluorescence-competent microscope technologies, further enabling researchers to discover and understand the intricate dynamics of subcellular biology and their detailed mechanics at ever-higher spatial and temporal resolutions (Figure S1).

The rapid advances in the field of fluorescence microscopy have required a collaborative effort; from physicists and engineers developing microscopy hardware, to chemists that continually develop and refine novel fluorescent probes, and biologists who utilise these tools to investigate the biological functions of diverse specimens. A misunderstanding of some of these disciplines by researchers from other areas often leads to poor experimental design and research outcomes. This review aims to summarise the three main considerations when fluorescence microscopy experiments are employed: (1) current hardware availability; (2) the different biological models applicable for fluorescence microscopy; and (3) the plethora of fluorescent probes available. The advantages and limitations for each factor will be discussed to allow the reader to make informed decisions when contemplating

experimental design. A helpful flowchart (Figure 1) is also provided to facilitate researchers to select the most appropriate combination of hardware, biological system, and imaging agent to achieve the best possible outcome in their imaging experiments.
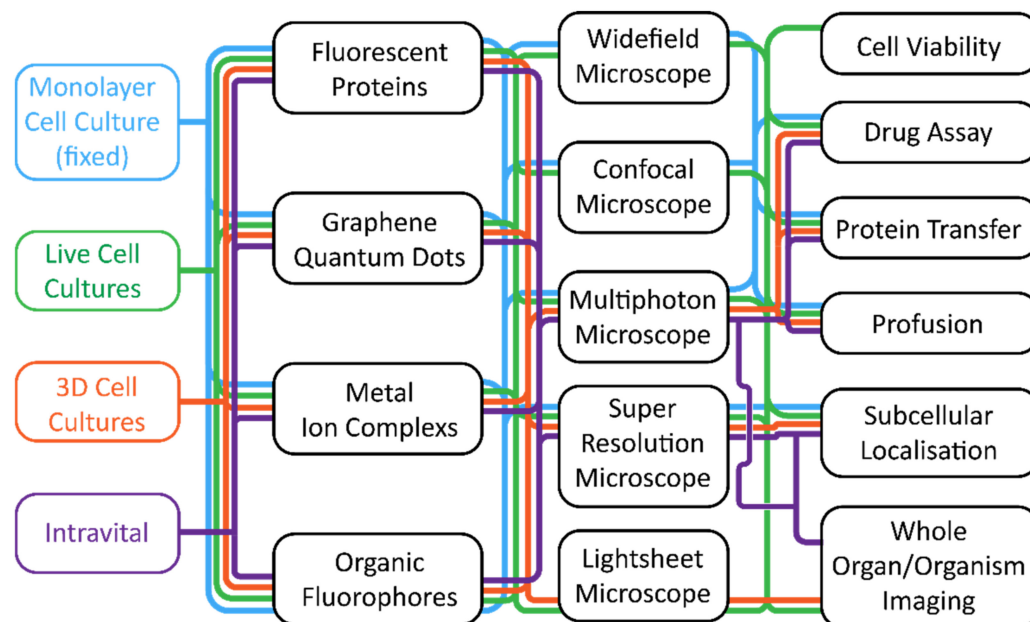


**Figure 1.** A flowchart linking biological systems to hardware combinations and applications. This flowchart should be read either from left to the right, working from the biological system to the desired application, or from right to left, where the application is chosen first. The flowchart is colour coordinated, and a chosen biological system will use the same colour throughout (blue for monolayer cell cultures, green for live cell cultures, orange for 3D cell cultures, and purple for intravital systems).

## 2. Fluorescence Microscope Hardware Systems

Widefield epifluorescence microscopes, established during the early 20th century, represent the fundamental type of fluorescence technology [1]. Many incremental improvements have been made over the years, both to the efficiency of the optics, as well as excitation sources and detection systems/cameras. These fluorescence microscopes are still widely used and are amenable to a wide range of applications, including evaluating expression rates of fluorescent tags and visualising whole tissue mounts.

Confocal microscopy represents a next step in fluorescence microscopy, offering higher spatial resolution, with the ability to visualise subcellular details, which are unachievable by conventional widefield systems. Invented by Minsky in 1955 [5,6], the confocal microscope makes use of lasers to raster scan an image to a point detector, and with a pinhole, blocks unfocussed light from the imaging plane, enabling optical sections of samples to be imaged [7]. This forms the basis of other models of laser scanning microscopes, which are tailored to specific applications.

### 2.1. Multiphoton and Other Advanced Microscopy Techniques

Modifying the laser excitation source of a confocal microscope with an ultra-fast pulsed laser enables two- or three-photon microscopy [8]. Ultra-fast lasers allow deeper penetration of samples using longer excitation wavelengths, and optical sections are created through confinement of the two (or multi) photon effect to a single focal plane. This technique is suited to imaging large tissue samples, where penetration depths of 100 μm or more are needed to investigate macro-scale biological processes. Multiphoton microscopes are also needed for intravital imaging, where both gentle illumination and imaging depth are critical for imaging live whole organisms. However, multiphoton microscopes are

limited by the added expense of purchasing an additional ultra-fast laser, which can add significantly to the cost of ownership and operation.

Laser scanning microscopes have been adapted to observe dynamic events in cellular function and exploit the properties of imaging probes, such as fluorescence lifetimes, and their interactions within and between cells. The three most common technologies employed are fluorescence lifetime imaging microscopy (FLIM) [9], fluorescence resonance energy transfer (FRET) [10], and fluorescence recovery after photobleaching (FRAP) [9]. FLIM requires the observation of intensity changes in a fluorophore over a course of time, which has been useful for quantifying decay rates of cell metabolites [11]. FRET measures energy transfer from one fluorophore to another using a single excitation, which allows for a variety of applications, such as calcium imaging [12] and protein–protein interactions/transfers [13]. Finally, FRAP measures the recovery in signal of a molecular probe after photobleaching, which enables the observation of diffusion kinetics in both cells and tissue samples [14].

Another recent technique, used to image larger tissue samples quickly and efficiently, is light-sheet fluorescence microscopy (LSFM) [15]. Light-sheet microscope operation differs from confocal microscopy, as samples are excited using a sheet of light from the side, as opposed to a focussed beam of light from the top or bottom of a sample. Emitted light is then detected perpendicular to the excitation sheet, unlike a confocal microscope, which detects the emitted signal in the opposite direction to the excitation beam. The thickness of the sheet of light determines the thickness of the optical section captured, and the sample can be rotated and moved through this plane to produce a three-dimensional tomographic image. Light-sheet fluorescence microscopy enables imaging of larger, multicellular samples, such as organoids and whole organisms (e.g., insects, plants, and animals [16–18]) that may not be adequately captured in a timely manner using single or multi-photon microscopy, although this does require tissue-clearing methodology to create optically transparent samples [19–21].

### 2.2. Super Resolution Microscopy (SRM); Going beyond the Limits of Light

Improvements in laser scanning microscopes have enhanced imaging resolutions beyond Abbe's limit (Equation (1)), the physical limitation due to the physics of diffraction, for example, a 200 nm resolution limit in air when using an excitation wavelength of 400 nm [22]; however, compromises such as hardware cost, phototoxicity, and low capture speed, remain limitations. The simplest technique to improve resolution using a confocal microscope is to restrict pinhole size, perform a z-stack, which involves combining multiple images captured at sequential focal planes, and perform post-processing of images using software deconvolution. However, acquiring a suitable z-stack of images involves repeated laser excitation, which significantly increases both cellular phototoxicity and the time to capture the complete micrograph [23].

$$d = \frac{\lambda}{2n \sin \theta} = \frac{\lambda}{2NA} \tag{1}$$

Equation (1) is Abbe's formula for the resolution limit, where $d$ is the minimum distance that can be differentiated between two points, $\lambda$ is the wavelength of light, $n$ is the refractive index of the medium the light is traversing, $\theta$ is the angle at which the light is converging, and $NA$ is the numerical aperture [22].

Another approach to improve resolution is stimulated emission depletion (STED) [24], which makes use of two lasers; one for excitation, and the other shaped into a ring or doughnut, used as a de-excitation or depletion spot to limit the size of the emitted fluorescent spot. STED typically improves resolution to 100 nm in all three axes, but this has compromises with phototoxicity and a lack of compatibility with conventional fluorophores and involves an increase in system cost.

A unique hardware addition by ZEISS to improve image resolution involves the use of an AiryScan detector in their confocal microscopes [25]. The AiryScan uses an array of

detectors laid out in a honeycomb pattern, which retains the light collection sensitivity of a conventional confocal microscope but enables an increase in resolution of approximately 1.4-fold without modifications to sample preparation. The compromise for this enhanced imaging technique is currently the increased hardware cost, and acquisition and processing time; the latter of which improves with continuous computational advances [25,26].

Additionally, structured illumination microscopy (SIM) is a hardware-based solution to improve image resolution by up to two-fold [27]. SIM works by projecting a moving grid onto the sample and recording multiple images as this lattice moves, creating an interference pattern known as the Moiré effect [27]. Processing these images improves the resolution by a factor of two, and recently, further improvements to the image processing algorithm have enhanced this to an additional two-fold [28], providing a spatial resolution as low as 60 nm. An advantage of SIM technology is the use of digital cameras for detection, rather than single point detectors, enabling these microscopes to capture highly dynamic events at frame rates exceeding 100+ frames per second [29]. Although SIM has minimal phototoxicity effects, it is limited by light penetration to maximal depths of ~200 μm [30,31].

Turn-key SIM systems can have the capability of performing single molecule imaging using photo activated localisation microscopy (PALM) or stochastic optical reconstruction microscopy (STORM). PALM and STORM both rely on photoactivation of fluorophores, which is a complex and highly sample-dependent process. Utilising this photoactivation of the fluorophores, molecules can be made to "blink" at differing time points and localities. Multiple images can then be acquired, and together with specialised algorithms, these images can be processed to achieve resolutions as low as 20 nm [32]. However, the current hardware cost of SIM systems limits their widespread adoption.

Microscope hardware is ever-evolving to suit the needs and applications of cell biologists. With steadily improving flexibility, sensitivity, resolutions, and speed, many historical challenges have been overcome, opening opportunities for further exploration and discovery. The key challenges are to minimise the trade-offs associated in choosing specific solutions, particularly with speed, resolution, phototoxicity, and imaging depth. To help the reader better understand the options available, we have compiled a detailed and useful table which compares the microscope types with respect to their advantages and limitations (Table S1).

### 3. Biological Models for Fluorescence Imaging; from the Monolayer Culture to the Whole Organ

The improvement in microscope technology allows biologists to employ a range of suitable models for the investigation of cellular mechanics. Cell culture plays a pivotal role in many fluorescence microscopy applications, where cells can be imaged from monolayers to three-dimensional (3D) cultures, such as spheroids, organoids, and tissue section explants, or extended to in vivo intravital imaging on living animals. In this section, we discuss the requirements and caveats of cell/tissue culturing to optimise the potential for imaging.

*3.1. Monolayer Cell Culture*

There are over 4000 well-characterised, readily available cell lines serving as models for human disease and development, which can be studied by researchers using a variety of imaging applications. Cell culture systems provide several advantages as models of more complex biological systems, including their potential for high-throughput screening, reproducibility, cost-effectiveness, reduced ethical considerations, well-documented protocols, and their ability to be easily manipulated. For example, cells can be transiently or stably transfected to introduce a gene of interest, enabling visualisation of a given protein using fluorescent protein tags. Cell lines offer an isolated monoculture of a single cell type, or co-culture of multiple cell types, which typically takes the form of a thin adherent monolayer or suspension culture [33,34]. For adherent cells, a uniform monolayer permits improved light penetration for imaging and consistent staining/immunolabelling, without

the need to permeate dyes and antibodies into deeper layers of a sample. This reduces sample-sample variability, providing more reproducible imaging results. Moreover, cultured cells exhibit less endogenous fluorescence, which can interfere with label detection, compared to processed tissues and organs [35], and do not require time-consuming tissue processing for imaging. A microscope equipped with an incubation system enables real-time visualisation of live cells [36] and time-lapse imaging [19], with minimal interference to normal cellular function due to environmental disturbance.

Microscopy using cell line models enables the exploration of subcellular processes that are implicated in disease pathogenesis, as well as cellular responses to therapeutics [37–39]. Whole cell imaging of two-dimensional (2D) cultures allows the examination of cell morphology [40] and intercellular communication networks, mediated by structures such as filopodia or cytonemes [41], tunnelling nanotubes [42], and cellular bridges [43]. Live cell imaging of cell cultures also enables the study of dynamic cell behaviour, such as extracellular vesicle formation, cell motility and migration in wound healing [44], and cancer metastasis [38]. Fluorescence microscopy of cell culture is also widely used to image subcellular components, including organelles and molecules, to provide greater insight into their structure, function, and subcellular localisation. Recent examples of the impressive details of cellular structures visualised by super-resolution microscopy (SRM) include nuclear pore complex organisation, membrane-associated periodic skeleton in neurons and synaptic structures [45]. Multispectral imaging, using confocal and lattice light-microscopy, revealed an intricate spatial-temporal organelle interactome in live cells [46], illustrating the usefulness of novel microscopy techniques to better understand complex cell biology.

Despite the benefits of cell culture models, several limitations need to be considered when examining cells by fluorescence microscopy. Live cell imaging, especially for prolonged time periods, requires the maintenance of viable cells under appropriate growth and culture conditions. Culture media are multicomponent solutions, containing various micro and macro elements, vitamins, proteins, fatty acids, and pH indicators, which can themselves be fluorescent or can interfere with the fluorescent properties of a given fluorophore [47]. For example, phenol red, present in most culture media, is fluorescent when excited at ~400 nm [47,48] and some vitamins (e.g., riboflavin and pyridoxal) increase photobleaching of GFP [49], while serum albumin can bind to some fluorescent probes to alter their spectral properties [50,51]. Concentrations of dyes also need to be carefully optimised to ensure specific staining of target structures or molecules. In addition, cells may respond to the fluorescent compounds, introducing artefacts that need to be considered and accounted for with appropriate controls. Likewise, the overexpression of fluorescently tagged proteins via transfection introduces artefacts into these cell models. As with all biological samples, cell cultures are highly susceptible to phototoxicity, and establishment of appropriate nontoxic detection settings is critical. With well-planned experimental approaches and appropriate controls, fluorescent imaging of cell cultures can be relatively simple and reproducible, providing a range of possibilities and techniques to study different processes and events at the cellular and subcellular level. Thus, the most significant drawback of this system is that cell culture models may fail to replicate in vivo biology, since they lack the complex network of interactions or intercellular signalling, which occur in tissues, organs, or whole organisms.

### 3.2. 3D Cell Cultures

The need for animal-free disease models that avoid the limitations of traditional cell culture monolayers, yet better mimic human in vivo environments and recapitulate the complex interactions between different cell types, has resulted in advances in 3D cell culture models. These can represent many tissues, including brain [52], breast [53], and prostate tissue [54], utilising scaffold or scaffold-free techniques to induce or cultivate their formation or maintenance. There are multiple types of 3D cultures, ranging from spheroids of cell lines to organoids derived from patient tissue (reviewed by Caleb and Yong [55]). Indeed, patient-derived organoids are utilised to offer personalised treatments and novel

therapeutic discoveries (e.g., [56,57]). Generated from cell lines cultures, spheroids or organoids may preserve the cell phenotypes observed in tissues, which result from interactions and responses to the microenvironment, such as detecting changes to necrotic tissue due to nutrient starvation in the centre of spheroids, mimicking rapidly growing non-angiogenic tumour tissue [58]. An example of the differences between 2D and 3D culture was demonstrated in cardiac cells; cells grown in 2D exhibited a large network of microfilaments and microtubules, whilst cells in a 3D environment were smaller in size, had many junctions between cells, and exhibited increased alpha actinin cytoskeletal protein [59]. Thus, 3D cell cultures may provide significant new insights into more complex cell biology, as well as disease biomarkers and therapeutics to improve translation.

Combining 3D cultures with 3D imaging is now being used to trace tissue development by stem cell differentiation and to determine responses to therapeutics. Recently, using a combination of immunohistochemistry and fluorescence microscopy, subpopulations of cancer stem cells were revealed to be affected in organoids via modulation of Wnt signalling upon Tankyrase inhibition [60]. These experiments were performed using morphometric analysis, with DAPI and F-actin fluorescence, to determine that the features that best described the compound-induced morphological changes are total organoid size, shape and size of lumen, live/dead cell counts, and changes in nucleus morphology [60]. Spheroid-derived image data are then used to produce characterisation methods that estimate growth and biophysical characteristics of multicellular tumour spheroids [61]. Using these spheroids, changes in cellular density and mechanical interactions are characterised, helping estimate cell diffusion, proliferation, and traction forces exerted by cells on the surrounding extracellular matrix [61,62]. The development of such protocols will be of significant benefit to the use of 3D culture in studying responses to therapeutics; however, there remains a need to investigate spheroids at a subcellular level to elucidate phenotypic changes occurring due to cell–cell interactions. Three-dimensional models have limitations for studying cell biology, as they still do not fully represent in vivo biology and, consequently, are still in development; as are the approaches to imaging these systems.

The ability to discover cell phenotypes and changes in disease processes, such as altered cell junctions, requires the use of fluorescence techniques to visualise subcellular protein location, expression, and distribution detectable by confocal microscopy. For example, trophoblastic cell spheroids have been utilised to investigate intracellular organisation and ciliary markers in cells starved of serum or treated with cytokines [63]. The accumulation of lipids and other light-scattering agents in multiple layers of cells within tissue presents a major hurdle to visualise the same biology in spheroids and organoids. Studies investigating extracellular matrix composition in spheroids [64] and evaluation of tight junctions in human intestinal organoids, have used cryosections [65] and immunohistochemistry to define the architecture and distribution of multiple markers (e.g., colorectal cancer [66] and corneal limbal organoids [67]). By performing serial sections, the structure may be re-created to reveal significant information about tissue; however, efficiency may be increased if antibody labelling and imaging could be performed on a minimally processed, intact organoid. To overcome the opacity of multiple cell layers, clearing methods can be used to render fixed spheroids and organoids transparent, through matching refractive index (RI) of the sample to increase transparency and allow more light penetration and reduced refraction. RI mismatches change the speed and angle penetration of light propagation onto cells, promoting light scattering, dispersion, and increased opacity [68]. For example, cell lipids and proteins have an RI value of ~1.44, whilst cytoplasm and nuclei have an RI of ~1.35 [69]. Hence, there are several optical clearing methods that aim to match the RI of the sample, increase sample transparency, and decrease light scattering to improve light penetration, imaging depth, and contrast [70]. Previously, these methodologies required long incubations of tissue, such as brain, for up to two weeks [71] or in toxic solvents [72]. However, new methods are being developed that are suitable for clearing spheroids more rapidly for higher-throughput protocols [73,74]. Our own analysis on prostate cancer spheroids has used a modified protocol from Ineveld et al. [74], and a

combination of urea, fructose, and glycerol, to image beyond 100 μm deep in spheroids, at a sub-micron pixel resolution. These improvements are, thus, likely to expand the use of 3D cultures for applications using fluorescence microscopy to study more detailed cell biology.

As light-sheet microscopy and multiphoton microscopy become more widespread, these techniques are likely to be the imaging options of choice for 3D cultures, due to their significantly improved imaging speed, light penetration, and reduced photodamage, compared to confocal microscopy [75,76]. These techniques also offer a significant advantage in that (in theory) commonly used fluorescence tools and protocols are applicable. Unfortunately, in practice, the application of many existing fluorescently labelled antibodies and dyes can be challenging to adapt to 3D cell culture systems, due to poor penetration of the often bulky molecules through multiple cell layers [76]. Transgenic cell lines containing fluorescent proteins can overcome this issue; however, this is not applicable when working with organoids grown from primary cells. As the use of organoids and 3D cultures becomes more common, we are likely to witness improved staining protocols and products to address these current challenges. The combined use of cleared and fixed organoids for high-resolution 3D analysis without the requirement of immunohistochemistry techniques, together with new label-free live cell imaging and 3D culture, is likely to become the standard for cell biology analysis in the near future.

### 3.3. Tissue Sections

A truer representation of in vivo biology is of course to take it directly from the source: tissue. The major advantage of using tissue sections compared to cell line models is that the complex interactions between a cell with its microenvironment are preserved, including the presence of the supporting extracellular matrix [77], the influence of stroma and immune cells [78], and the maintenance of cell polarity in the hierarchical architecture of the tissue [79]. The ability to collect a snapshot of in vivo biology and preserve this for future study is invaluable, and biobanks with archived tissue exist for a multitude of diseases.

Tissue samples can be sourced in two forms: formalin-fixed paraffin-embedded (FFPE) or frozen. FFPE tissue is the most common and accessible sample type, with tissue preserved by formaldehyde fixation and embedded in paraffin wax blocks. In this way, large tissue collections can be routinely processed, and easily stored at room temperature to remain viable for decades. Compared to FFPE samples, cryopreserved frozen tissue is a much more limited resource but has several unique applications. 'Fresh' frozen tissue is generally snap-frozen in liquid nitrogen or isopentane immediately after resection, while 'fixed' frozen tissue is either perfused with fixative before cryopreservation to better retain tissue morphology and protein antigenicity, or fixed after snap-freezing for downstream application. Tissue can be a relatively scarce and precious resource, especially human tissue, which needs to be either sourced from biobanks, collected post-surgical removal, or obtained from animal models for disease. In all cases, gaining access to human or animal tissue can often be a costly and time-consuming endeavour, which is why cell culture can be an attractive alternative despite its discussed drawbacks. However, the ability to study tissue with all its complexity is invaluable and well worth the exertion.

Protocols for many applications exist for use on both frozen and FFPE tissue sections, and the choice of sample is a compromise between many factors. FPPE tissue is routinely collected in diagnostic labs and the process of embedding in paraffin maintains the integrity of the tissue architecture, making FFPE sections superior for morphological studies. However, non-standardised protocols between different institutions in tissue handling, fixation, and processing can create significant variability between samples with regards to background staining and analyte intensity [80]. A major concern with using tissue sections for fluorescence microscopy is inherent autofluorescence in the sample. Several components of tissue auto-fluoresce, including collagen [81], elastin [82], red blood cells, and some immune cells [35]. FFPE sections are more susceptible to this compared to frozen tissue, exacerbated by artefacts carried over from suboptimal fixative procedures or choice

of fixative [83]. In frozen samples, tissue constituents such as lipids, which are removed in most standard FFPE processing protocols [84], proteins, and nucleic acids, are preserved in their native states. FFPE tissue processing creates extensive cross-linkage of proteins, which may mask some protein antigens in their native state [85]. This makes frozen tissue useful for molecular analysis such as DNA sequencing [86] and study of post-translation protein modifications compared to FFPE in which these may be poorly preserved. This can be particularly advantageous for fluorescence in situ hybridisation (FISH), which uses a fluorescent probe to label and spatially map nucleic acids in tissue sections [87]. However, during the freezing process, ice formation within the sample can damage tissue morphology and this can create artefact with distortion of the tissue compromising morphological characteristics. These varying factors need to be carefully considered for each experimental application and what level of sample quality is required, for which there are many useful reviews discussing tissue artefact and comparing handling protocols [88–90].

Although imaging of both 3D cell culture and tissue sections are widespread in investigating cell biology, to date, most biological research relies on standard cell culture and ex vivo models that cannot fully recapitulate physiological conditions, sometimes leading to artefacts and inaccurate results [91,92]. Imaging of biological processes in the context of a living organism opens new avenues in biomedical research, allowing visualisation of cellular and molecular associations in real time in their natural environment. Intravital or in vivo fluorescent microscopy has become a quintessential tool in the direct visualisation of the biological processes in living animals, with significant applications in studying alterations in tissue morphology and function [93,94], redox dynamics [95], cell proliferation and differentiation [96,97], cell migratory behaviour [98,99], tumour microenvironment [100,101] reviewed in [102], intracellular ionic activity [103,104], and host–pathogen interactions [105].

### 3.4. Intravital Imaging

Intravital imaging requires access to a high-resolution confocal, multiphoton, and/or light-sheet microscope, and the development of suitable animal models. Transgenic animals modified to express fluorescently tagged proteins provide a true in vivo environment for evaluating various cellular processes, with constitutive replenishment of fluorescently labelled proteins enabling long-term tracing in a cell- and tissue-specific manner. This technique mainly makes use of small organisms, such as fruit flies [106–108], zebrafish [95,109,110], and mice [111,112], due to their short generation times, established genetic lines, and relatively low cost. Subcutaneous and orthotopic xenograft models used in intravital studies can accurately provide insights into tumour heterogeneity and responses to drug treatments [113,114]. With the use of intravital microscopy, it has also become possible to visualise the inter-individual variability at a microscopic level in response to drug treatment. An advantage of intravital imaging is the continual monitoring of physiological changes over days and weeks, which is especially important in developmental cells [97], stem cell [115,116], and tumour biology [117]. Moreover, longitudinal intravital imaging can be performed with fluorescently labelled antibodies and dyes that can be intravenously injected for the simultaneous visualisation of, for example, individual lipid droplets and microvasculature in the liver [118], or even vessels in the femoral and calvarial marrow [119]. Recent advances in optics have brought intravital imaging into a new era of high-resolution fluorescence microscopy. These include digital adaptive optics scanning light-field mutual iterative tomography (DAOSLMIT) that utilises computational imaging from tiled wavefront correction with high-speed and high-resolution multi-dimensional imaging with low phototoxicity [120], to enable longer and higher-speed 3D subcellular imaging, to better study intercellular and intracellular interactions in tissue. Likewise, FLIM-FRET imaging has recently been applied to intravital imaging of kidney to study metabolic changes in different cell types through the organ [121].

Although intravital imaging is a powerful tool to study various biological processes in live organs and animals, several challenges need to be addressed, including anatomical

constrains (i.e., organ accessibility), selection of appropriate techniques (e.g., type of incision and immobilisation of organ), and the use of inverted/upright microscopes (reviewed in [122]). Long-term imaging at a single-cell resolution in the cornea, skin, and hair follicles [123,124] does not require special preparation for obtaining optical access; however, small animals such as *Drosophila melanogaster* and zebrafish need to be anesthetised prior to imaging to permit the required surgical procedures to expose specific organs [106,109]. Accessing other organs of interest in larger animals such as mice is more challenging; the organ of interest can be surgically exposed, preserving its structure, connectivity, and perfusion in the anesthetised animal [125,126]. This invasive procedure may alter physiological homeostasis and can only be used for short-term imaging without impacting negatively on data for easily accessible sites, such as dermal vasculature [127], popliteal lymph nodes [128], salivary glands [126], small intestine [129], and liver [130]. Methods for imaging heart, kidneys, pancreas, and spleen are less developed and are at greater risk of artefacts that may result from inflammatory reactions. Long-term imaging of cellular processes requires installation of the optical windows adjacent to the organ of interest in a live anesthetised animal (reviewed in [131–133]), which permit unlimited microscope access to various abdominal organs [97,134], lungs [135,136], tumour-associated vasculature [137] and lymphatic vessels [138], spinal cord [139], and brain [140]. Although this technique allows visualisation of tissues/organs in their orthotopic location, implantation of the windows can lead to infections and motion artefacts. Moreover, animals can die during the surgery and the optical window can break or detach after successful implantation. These problems can be overcome by the use of optical fibres that provide access to sites deeper within the organ [141,142], or with micro-endoscopic probes employed to provide a less invasive observation mode of cellular-level features in colon [143,144], oesophagus [145,146], and trachea [147]. Fluorescent micro-endoscopy is a powerful technique for imaging the internal structure of a hollow organ; however, it can have a lower resolution and smaller field of view compared to high-resolution microscopes used in the techniques above. Furthermore, the physiological motion of the animal through respiration and cardiac activity can introduce significant imaging artefacts and compromise spatial information, particularly if the raw acquisition data remain uncorrected by special image processing algorithms [148,149].

Techniques and methodologies for intravital imaging are somewhat further advanced than those developed so far for 3D cell culture imaging. However, the methodologies still require expert knowledge and equipment to maintain animals during experimentation. In addition, ethical considerations need to be made when using these approaches, which go beyond those of standard animal experiments. Fluorescence microscopy of preserved tissue or organism post-mortem, therefore, is a more common approach when working with animal models. The challenges encountered when using fixed tissues or whole organisms mostly relate to sample thickness and fixation artefacts. As discussed above, tissue significantly hampers light and antibody/dye penetration, and requires further sample preparation, including sectioning and optical tissue clearing. The major drawback of imaging tissue post-mortem, when compared to intravital imaging, is the loss of dynamic processes and introduction of potential artefacts by surgical excision of the organ of interest and fixation processes. However, given the extensive use of animal models for biomedical research, the fluorescence microscopy of fixed animal tissues is widely used and has contributed significantly to our understanding of tissue morphology and molecular dynamics under normal and disease conditions.

## 4. Imaging Agents Used for Fluorescence Microscopy

Fluorescent labels are pivotal for fluorescence microscopy, allowing the detection and monitoring of a range of cell types and subcellular structures, which do not naturally fluoresce. Imaging agents are ideally water soluble and non-toxic species, which exhibit favourable photophysical properties, including large Stokes shifts, high quantum yields, resistance to photobleaching, long lifetimes, and excitation/emission properties amenable to commercially available hardware. There are four main categories of imaging agents for fluorescence microscopy applications: fluorescent proteins (FPs), graphene quantum dots (GQDs), metal-ion

complexes, and organic fluorophores. Each of these classes have their own set of advantages, limitations, and experimental considerations, as discussed below. Although other types of imaging probes exist, such as radio-labelled contrast agents [150–152] and nanoparticle formulations [153,154], we have not included these here, as they are more frequently used in imaging techniques outside of fluorescence microscopy, such as magnetic resonance imaging (MRI) [155], positron emission tomography (PET) [156], computed tomography (CT) [157], single-photon emission CT (SPECT) [158], surface-enhanced Raman scattering (SERS) [159,160], and planar scintigraphy [161]. The following sections are designed to provide a brief understanding of the outlined four categories, with the selected examples demonstrating their use in fluorescence microscopy and the biological system/hardware conditions employed. This section also highlights the need for effective collaborative interactions between chemists, biologists, and physicists to solve critical problems in fluorescence imaging.

### 4.1. Fluorescent Proteins

The discovery of GFP in 1962 [162], and its subsequent cloning 30 years later [4], has led to FPs becoming an integral tool for cell biologists to monitor cellular processes using fluorescence microscopy. Since that time, a variety of FPs have been synthesised, which traverse the visible spectrum and have been well covered in some excellent reviews [163,164]. Fluorescent proteins are large molecules (typically 25–30 kDa) that exhibit bright fluorescence and excellent bioavailability [163]. The main point of difference between FPs and the other imaging strategies reviewed below is how they are applied. Typically, the FP is introduced into a cell via genetic encoding to express as a fusion tag to a protein of interest, as opposed to applying an exogenous labelling agent. Transfection obviates any cellular penetration issues, which can be experienced by other probe types [165]. Furthermore, this approach inherently allows for quantitative imaging as FPs can be expressed in a 1:1 ratio with their target substrate [166].

The impact that genome coding can have on the normal operation of the cell should always be a consideration. For example, cells transfected with enhanced GFP (eGFP) have been shown to trigger the proliferation of harmful reactive oxygen species [167]. The large size of FPs also need to be considered with respect to perturbation of normal functioning of the endogenous protein [168] and the over-expression of FPs, which can lead to aggregate formation [169,170]. Inaccurate interpretation of protein distribution and function resulting from these issues should be carefully controlled for in the experimental design. The robustness of FPs can vary considerably with construct purity, labelling [171], and excessive background fluorescence [172]. Typically, FPs are unable to image acidic environments [173,174]; however, examples do exist where this property has been exploited. For example, Trejo and co-workers used a pH-sensitive GFP (pHluorin-mKate2) to monitor starvation-induced autophagy in LC3B transgenic mice, where the FP was non-fluorescent in acidic compartments, but was emissive in neutral or basic environments [175].

A major disadvantage of FPs is their high background fluorescence, which can make the processing of images difficult. To circumvent this issue, FPs have been designed where a non-fluorescent protein becomes emissive upon activation by a trigger [176]. A recent example from Wu et al. reported the use of FPs, which bind to RNA aptamers to evoke a "turn-on" fluorescent response and allow visualisation of mRNA in live HEK293 cells using an epifluorescence inverted microscope [177]. This approach significantly improved background fluorescence when compared to the more traditional MS2-MS2 coat protein (MCP) tethering approach used to image mRNA [178–180]. Other examples have adopted this approach to image RNA trafficking [181,182].

Simultaneous expression of several FP markers allows multicolour labelling of cellular process, compartments, or proteins of interest to be investigated in parallel within a cell. The "Brainbow" strategy relies on a handful of spectroscopically distinct FPs to provide information of different cellular types and environments, by emitting a broad palette of detectable hues [183]. Hematopoietic stem cells, which give rise to B and T cells, have recently been imaged by transplanting a range of fluorescently labelled cells with differing emission profiles, to provide information on hematopoietic cell lineage in Rag1$^{-/-}$ mice

using confocal microscopy [184]. Similarly, live pluripotent stem cells were imaged by confocal microscopy to track their eventual derivatisation using the Brainbow technique (Figure 2) [185]. This approach has recently been supplemented with a secondary near-infra red FP (mCardinal), whose expression is driven independently of the Brainbow cassette [186]. This novel combinatorial system opens the door to further expand the Brainbow and related multi-colour techniques of FPs.
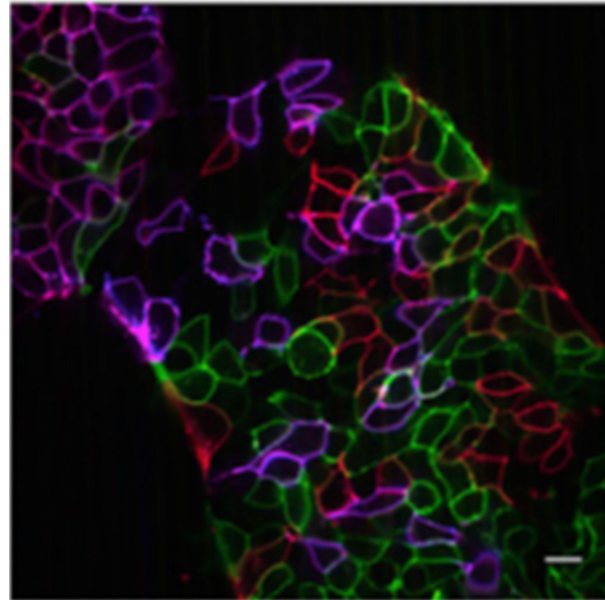


**Figure 2.** Live human-induced pluripotent stem cells after 12 h with transfected with eGFP, mOrange2 and mKate2. Scale bar = 20 μm. Reproduced with permission [185]. Copyright 2020 Elsevier.

　　　Despite the considerable effort to construct new FPs with different optical parameters, the field is still largely limited by spectral overlap between their broad fluorescence profiles [187,188]. This characteristic of fluorophores is taken advantage of in applications such as FRET. A recent example of a FP-based FRET system was reported by Shen et al., who created three independent potassium ion ($K^+$) sensors to measure both intra and extracellular $K^+$ [189]; a critical electrolyte for cell function [190]. This was achieved in live HeLa cells using confocal microscopy. The overall design of each system (Figure 3) relied on a "turn-on" effect when two potassium binding proteins encapsulated $K^+$, which brought the FRET donor and acceptor FPs close enough to elicit a FRET response. FRET sensing is also widely used to monitor protease activity by coding FPs linked together by a protease-specific cleavable site, leading to a "turn off" effect. This strategy has been used to measure common proteases such as Caspase-3 [191,192], Trypsin [193,194], Thrombin [195,196], and Calpain [197,198]. FRET-based systems continue to be an area of interest to extend emission into the near-IR part of the visible spectrum, by tailoring FP donor and acceptor photophysical properties [199,200]. The main advantage of using FPs for FRET imaging is that the fluorescent donor and acceptor are produced by the cells, which obviates the need for small molecule labelling and issues encountered with cellular penetration. Excluding these specialised uses, overlapping excitation-emission profiles remain an issue when using FPs, and a judicious selection of fluorophores is required to maximise photophysical potential of the system and to limit unwanted behaviour alterations of the fusion protein from coding in the FP genes [171,173,201].
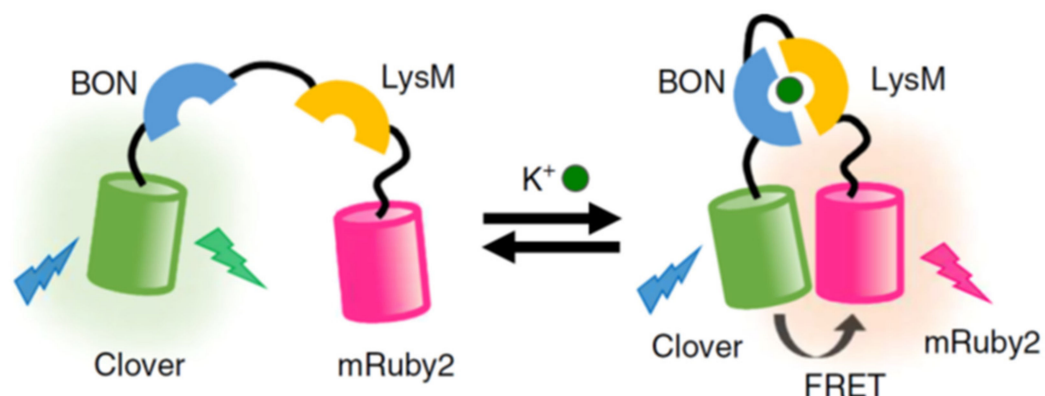
**Figure 3.** Schematic of the KIRIN1-GR FRET system where emission at a higher wavelength is detected after potassium binding. Image adapted with permission [189]. Copyright 2019 Springer Nature.

The ability of fluorescent proteins to be genetically encoded into a cell as a non-invasive fluorescent tag, without the need for fixing or permeabilising cells, makes them indispensable for live cell imaging, and may be increasingly useful in 4D imaging of opaque samples such as spheroids [202], where the penetration depth of antibodies and dyes may be limited. Imaging in four dimensions can shed light on intracellular dynamics, such as protein trafficking and organelle interplay [203], and has also been applied to small single-celled systems such as yeast [204]. For example, fast 3D-phase imaging combined with 3D super-fluorescence microscopy has allowed the imaging of actin filaments in live RAW 264.7 macrophages transfected with the Lifeact-Dreiklang FP [205]. Another recent example uses fluorescence correlation spectroscopy to generate high-throughput quantitative 4D images for a range of counting applications; this method can be used with effectively any monomeric FP such as mCherry and mScarlet [206]. The advantages of using FPs for 4D imaging is proving to be a hot topic, and we expect significant growth in this area as the technology continues to be developed.

*4.2. Graphene Quantum Dots*

Graphene quantum dots (GQDs) are zero-dimensional fluorescent nanomaterials that have been exploited for a variety of imaging and sensing applications. This category of imaging technology is the most recent of the classes reviewed here; however, their potential for greater use in fluorescence microscopy is significant with a surge of recent examples within the literature. We have focussed on GQDs rather than other varieties of inorganic QDs, which often suffer from solubility and toxicity issues owing to their reliance on incorporated heavy metals such as cadmium, mercury, and lead [207,208]. Conversely, GQDs are water soluble materials which have excellent toxicity profiles [209–211]. The photophysical properties of GQDs are amenable to fluorescence microscopy with higher molar absorptivity coefficients, improved photostability and longer-lived emission compared to organic fluorophores [208]. A major advantage of using GQDs is how easily they can be synthesised using either a 'top-down' or 'bottom-up' approach [212–214]. Of these two strategies, the 'bottom-up' approach has become the favoured route, given starting material affordability and the simplicity of the method, which does not require specialist chemistry or cellular biology training, unlike other imaging strategies reviewed here.

A drawback of using GQDs is that by virtue of their synthesis, a heterogenous and inseparable mixture of chemical structures is formed, which inherently makes characterisation difficult when using traditional analytical techniques employed for small molecules, such as NMR spectroscopy and mass spectrometry [215]. As a result, techniques such as IR, XPS, and UV-visible spectrophotometry are relied on to characterise the bulk material. This structural ambiguity means that functionalisation of the GQD surface is also more difficult when compared to organic fluorophores, as the exact number (and sometimes type) of reactive handles are unknown and reaction monitoring is almost impossible. Nonetheless,

advancements have been made with several successful functionalisation strategies having been summarised in review articles [215,216].

Initially, GQDs were explored for their viability as cellular imaging agents by evaluating toxicity, cellular uptake, and visualisation on a range of cells [217–219]. Once it was apparent that these materials were amenable to such endeavours, more sophisticated systems were designed. For instance, pH sensing in HeLa cells using folic acid-encapsulated GQDs has been reported, where a pH increase from 5–8 results in an increase in emission intensity in the green detection window (500–570 nm, $\lambda_{ex}$ 488 nm), using confocal microscopy, while the emission intensity in the blue detection window (425–490 nm, $\lambda_{ex}$ 405 nm) remained relatively unchanged (Figure 4) [220]. A more recent example has used nitrogen-doped GQDs to detect temperature in live HeLa cells by measuring the temperature-dependent fluorescence quenching as the cells are warmed from 25–45 °C [221].
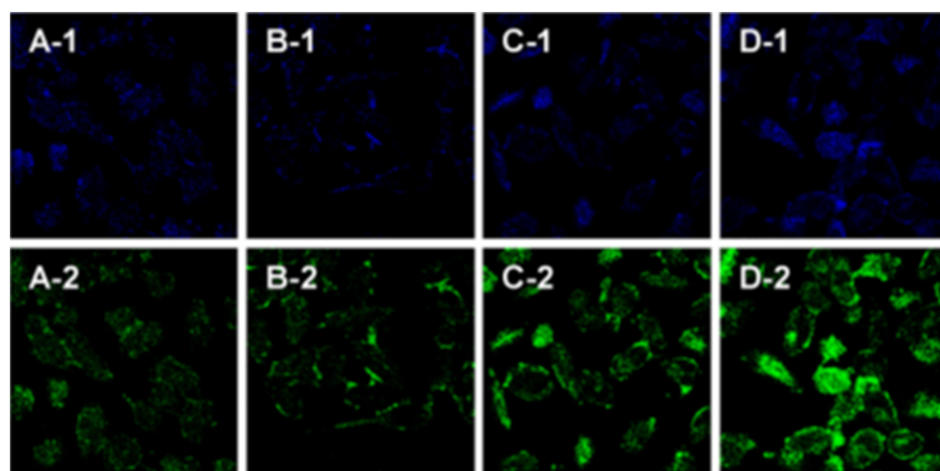


**Figure 4.** Confocal micrographs of HeLa cells incubated with 1 mg mL$^{-1}$ folic acid-encapsulated GQDs for 6 h at various pH (5, 6, 7, and 8; **A**, **B**, **C**, and **D** respectively). **1** (425–490 nm, $\lambda_{ex}$ 405 nm) and **2** (500–570 nm, $\lambda_{ex}$ 488 nm) refer to the different spectral windows. Reproduced with permission [220]. Copyright 2018 Elsevier.

The detection of mercuric ions (Hg$^{2+}$) in living cells is an important pursuit given the high toxicity they impart on the body, which can lead to kidney, liver, and brain damage [222]. GQDs coated with thymine-rich DNA have been reported to accurately detect Hg$^{2+}$ in HeLa cells, whereby Hg$^{2+}$ strongly coordinates with thymine residues to create a rigid hairpin on the GQD surface, ultimately decreasing the GQD emission at 460 nm by approximately 90%, as observed using confocal microscopy [223]. Another example of intracellular Hg$^{2+}$ detection utilised GQDs conjugated with rhodamine fluorophores to create a FRET 'turn-on' system in the presence of Hg$^{2+}$ (Figure 5). The FRET construct demonstrated excellent reversibility (up to five cycles) and good biocompatibility in HeLa cells [224]. Other metals have been successfully detected in live cells using GQDs too, including a ratiometric GQD-Nile Blue conjugate for two-photon detection of Cu$^{2+}$ ions in A549 cells [225] and nitrogen-doped GQDs, which could reversibly detect Al$^{3+}$ and had demonstrated imaging capacity in HeLa cells [226]. The sensing of non-metal ions critical in biological systems has also been achieved using GQDs. For instance, nitrogen-doped GQDs were used to detect nitrite (NO$_2^-$) as low as 2.5 nM in live human bladder carcinoma T24 cells, using laser scanning confocal microscopy, with no cytotoxicity and good biocompatibility observed [227]. Hypochlorite (ClO$^-$) is a vital ROS species endogenously produced in living organisms from hydrogen peroxide (H$_2$O$_2$). GQD sensors capable of detecting both of these chemicals in cells have been reported, with GQDs furnished with *o*-phenylenediamine units capable of detecting ClO$^-$ at 69 nM in MCF-7 cells [228], and a FRET-based system employing a GQD conjugated with boronate merocyanine chromophore-efficient H$_2$O$_2$ reporters in HeLa cells using two-photon excitation [229].
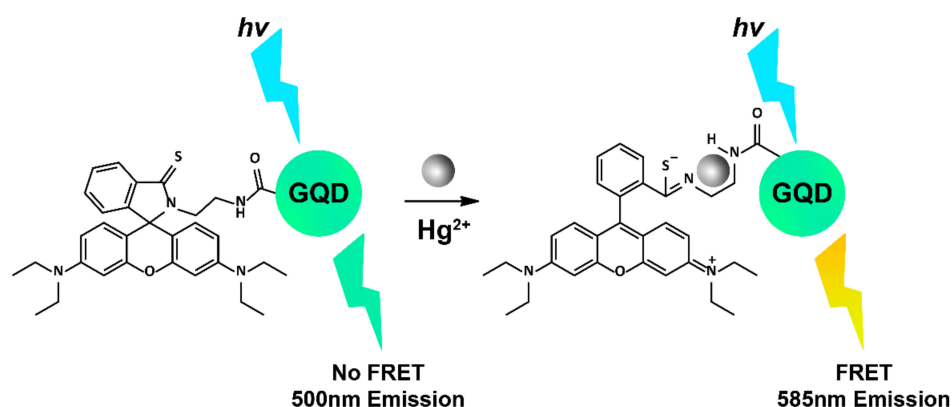
**Figure 5.** Proposed FRET mechanism of rhodamine-GQDs detecting $Hg^{2+}$. Image adapted with permission [224]. Copyright 2015 Elsevier.

Defining subcellular structures is a common goal in fluorescence microscopy and tools that allow this level of specificity are much sought after. Although this domain is mostly owned by organic fluorophores, GQDs have been utilised to track subcellular components too. For example, GQDs were functionalised with ethylenediamine groups (via an acid chloride route) to generate a probe which selectively stained the nucleolus in live HepG2 cells, as evidenced with co-staining experiments with the commercially available SYTO RNA-Select nucleolus stain [230]. The mitochondria has also been successfully targeted using a ratiometric GQD-cyanine conjugate FRET system, which is specific for mitochondrial peroxynitrite ($ONOO^-$) and can detect $ONOO^-$ at concentrations as low as 30 nM, as evidenced using laser scanning confocal microscopy on RAW264.7 cells [231]. Protein conjugation in order to monitor uptake and trafficking behaviour can also be studied using GQDs, as has been achieved with insulin-conjugated GQDs used to monitor insulin receptors in live 3T3-L1 adipocytes, confirmed by co-staining experiments (Figure 6) [232]. A similar concept was reported for tracking transferrin receptors with transferrin conjugated GQDs to monitor real-time imaging in HeLa cells [233].
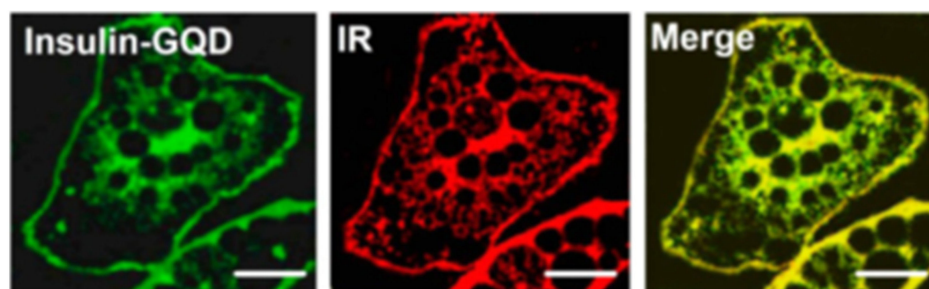


**Figure 6.** Confocal fluorescence images of fixed 3T3-L1 adipocytes. (**left**) Cells are stained with Insulin-GQDs; (**middle**) cells are treated with antibodies against insulin receptor B subunit followed by Atto647 NHS-conjugated secondary antibodies; (**right**) merged image to demonstrate insulin receptor staining. Scale bar = 10 μm. Reproduced with permission [232]. Copyright 2013 American Chemical Society.

Tools which can differentiate between cell and organ types are valuable in bioimaging applications. Although GQDs are still emerging as a viable option for these types of studies, there have been a handful of examples that clearly demonstrate their potential in this field. For example, in mice, near-infrared emitting GQDs were shown to preferentially localise in the kidney and liver, when compared to other organs [234]. A more sophisticated example has been recently published with $Nd^{3+}$ and $Tm^{3+}$ (rare earth metals)-doped GQDs used to image mice, with maximal uptake observed in the kidneys, liver, spleen, and intestine, using fluorescence microscopy [235]. Additionally, GQDs that exhibited emission in the

yellow region of the visible spectrum showed efficient staining of stem cells when excited at 405 nm [236]. This type of work has naturally been extended into the theranostic and drug delivery space with GQDs finding use in targeting breast cancer [237], pancreatic cancer [238], and the delivery of Doxorubicin to HeLa cells [239]. For instance, GQDs decorated with hyaluronic acid moieties to enhance cancer cell uptake were used as drug carriers to deliver curcumin as a drug model to HeLa cells, where it was released upon exposure to the mildly acidic environment of the cancer cells. Consequently, this system imparts good selectivity with no toxic effect observed on normal cells [240].

*4.3. Metal Ion Complexes*

Metal ion complexes have been successfully used in cellular imaging applications such as subcellular compartment staining and visualisation of cellular processes. A variety of sensitising pathways have been utilised for these types of metal complexes, such as metal-to-ligand charge transfer (MLCT) and ligand-to-ligand charge transfer (LLCT), which have been reviewed previously [241]. The major advantage of using metal ion complexes as imaging agents are their long-lived emission profiles, which facilitate the use of time-gated fluorescence microscopy experiments, such as FLIM, and enables the visualisation of cellular events, which is otherwise not possible due to endogenous autofluorescence within cells [242]. Moreover, metal ion complexes offer highly tuneable excitation and emission profiles, which span the entire visible and near-IR spectrum. They also offer the largest Stokes shifts of the four classes covered in this review (typically greater than 5000 cm$^{-1}$), which obviates self-quenching issues encountered by most organic fluorophores [243].

Metal ion complexes are still considered small molecules (when compared to much larger GQDs and FPs); however, their structures are typically more complex compared to organic fluorophores, which renders their synthesis more difficult. The metal core can often impart cytotoxic effects, which can limit their use in live cell imaging applications [244] and lead to poor water solubility making handling difficult. Despite these drawbacks, metal ion complexes have been successfully used for a range of live cellular imaging applications.

Metal ion complexes for cellular imaging can be divided into two main sub-classes; low-spin d-block transition metals with $d^6$, $d^8$, or $d^{10}$ electronic configurations, such as Re(I), Ru(II), Ir(III), and Pt(II), and f-block emissive lanthanoids, such as Ln(III), Eu(II), Gd(II), and Tb(III) [245]. Re(I) carbonyl complexes are the most common type of transition metal complex used in bioimaging [246], as they can be readily functionalised to serve a required purpose. For example, Amoroso and co-workers have reported two similar Re(I) tricarbonyl metal ion complexes with either hydroxymethyl or chloromethyl substituted pyridinyl ligands, which exhibit vacuole and mitochondrial localisation (**1** [247] and **2** [248] respectively, Figure 7). More recently, the Massi group has contributed to this area with a range of Re(I) complexes including **ReZolve-L1** featuring a benzonitrile group [249], which was the first report of a selective dye for polar lipids in live cells [250], and a pyridinyl substituted derivative (**ReZolve-ER**), which localises within the endoplasmic reticulum (ER), both evidenced using confocal microscopy [251].

The Massi group have also conducted a thorough investigation of Ir(III) complexes and how a subtle structural change, from a neutral tetrazole group (**[Ir(ppy)₂(TzIQn)]**, Figure 8) to a methylated cationic tetrazole (**[Ir(ppy)₂(MeTziQn)]⁺**), can impart significant cellular uptake properties with H9c2 staining observed in the ER and mitochondria, respectively [252]. Interestingly, the cell uptake of these compounds was independent of lipophilicity. Conversely, another set of Ir(III) complexes have been reported whose toxicity and cellular uptake is strongly dependent on the lipophilic character of the probe (**3**, Figure 8) [253]; this is clear evidence that metal ion complexes need to be assessed on a case by case basis for cellular imaging capacity. Another example of how lipophilicity impacts cellular staining has been demonstrated using morpholino-conjugated Ir(III) complexes with varying LogP values. The morpholino group has been successfully used to target lysosomes for Ir(III) complexes in the past [254]; however, **Ir1** preferentially localised within the mitochondria (87% Pearson's correlation coefficient with MitoTracker™), while the

less hydrophobic **Ir5** was observed in the lysosome (79% Pearson's correlation coefficient with LysoTracker™) [255]. These morpholino-conjugated Ir(III) complexes were further explored by adding a third morpholino group to improve water solubility and allow for two-photon excitation of long-lasting lysosome imaging in HeLa cells [256]. Other examples of Ir(III) complexes have been reported to sense changes in the mitochondrial environment, either for hypoxic conditions [257] or labile $Zn^{2+}$ ions [258]. There are also examples of Pt(II) [259,260] and Ru(II) [261,262] metal ion complexes for cellular imaging; however, these are less favoured options when compared to the Re(II) and Ir(III) alternatives, presumably owing to their comparatively weaker photophysical properties. Moreover, transition metal complexes have been used for sensing purposes too, including endogenous nitric oxide [263] and thiol [264] sensing using Ru(II) complexes.

Trivalent metal ions from the lanthanide series of f-block elements have also shown extensive application for cellular imaging. These systems nearly always rely on an antennae group to populate the metal excited state, which gives rise to the characteristic phosphorescence signal exhibited by the lanthanide ion [243,265,266]. Additionally, these complexes require a chelator to affix the lanthanide ion in a position whereby energy transfer can take place. A wide range of ligand/chelator/lanthanide ion combinations have been reported and are well-reviewed [265,267]. Lanthanide complexes are normally used for the tracking of key biological processes or key biomolecules, rather than staining specific regions of the cell. For example, the concentration change of adenosine triphosphate (ATP) within the mitochondria has been measured effectively using cyclen-Eu(III) complexes, such as that shown in Figure 9. The quinoline arms of the complex likely aid in the Eu complexation and the pendant amide groups are proposed to aid in ATP binding. This was demonstrated in NIH-3T3 cells to provide real-time measurement of ATP in live cells by a 'turn-on' luminescent effect, using laser scanning confocal microscopy [268]. A similar design concept reports a lysosomal targeting Eu(III) complex for hypochlorous acid sensing in live RAW 264.7 cells, using time-gated luminescent imaging [269].
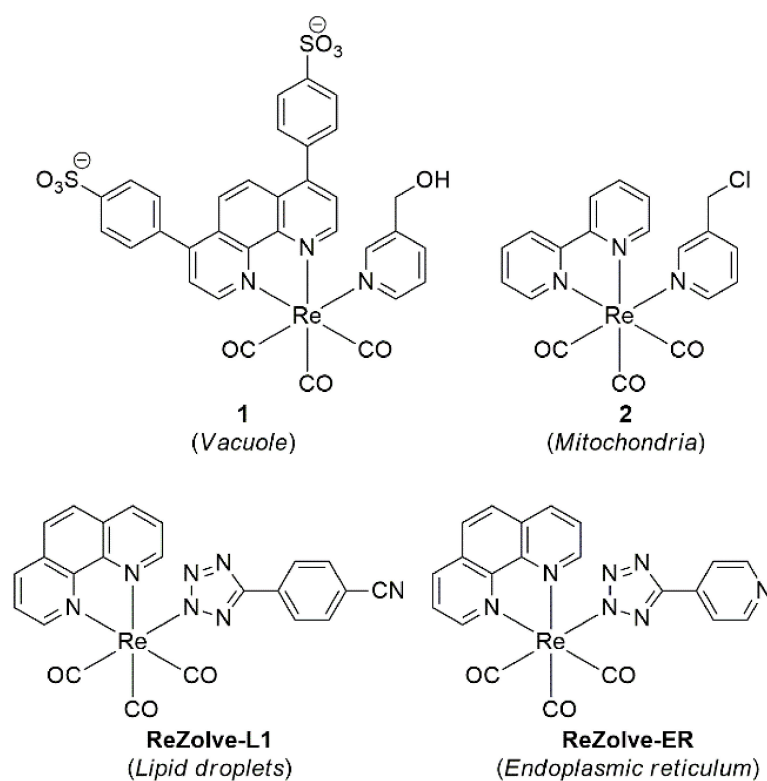


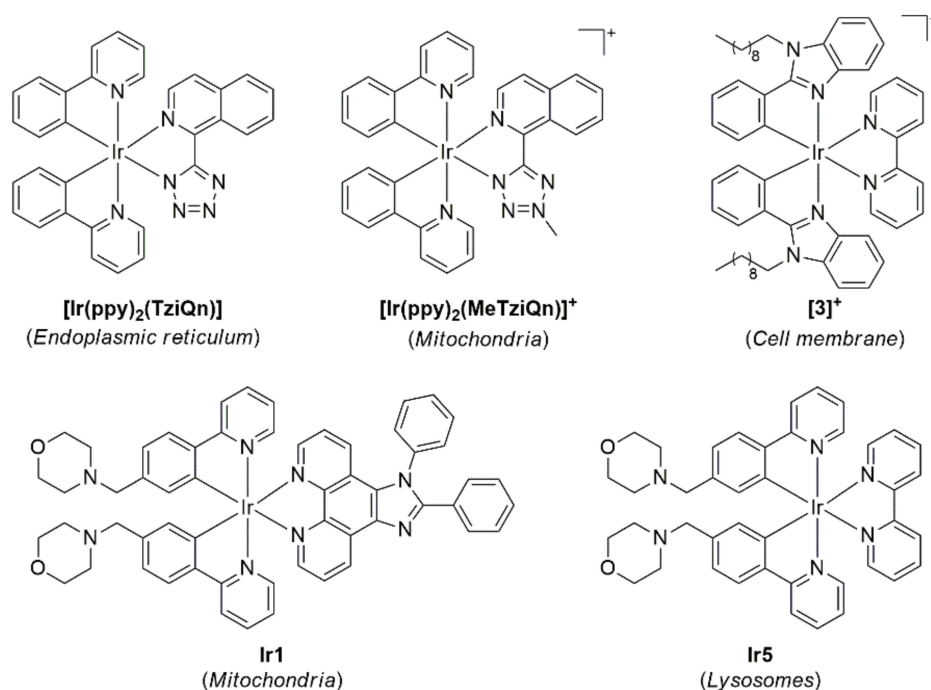**Figure 7.** Reported Re(I) complexes with organelle localisation in parentheses.

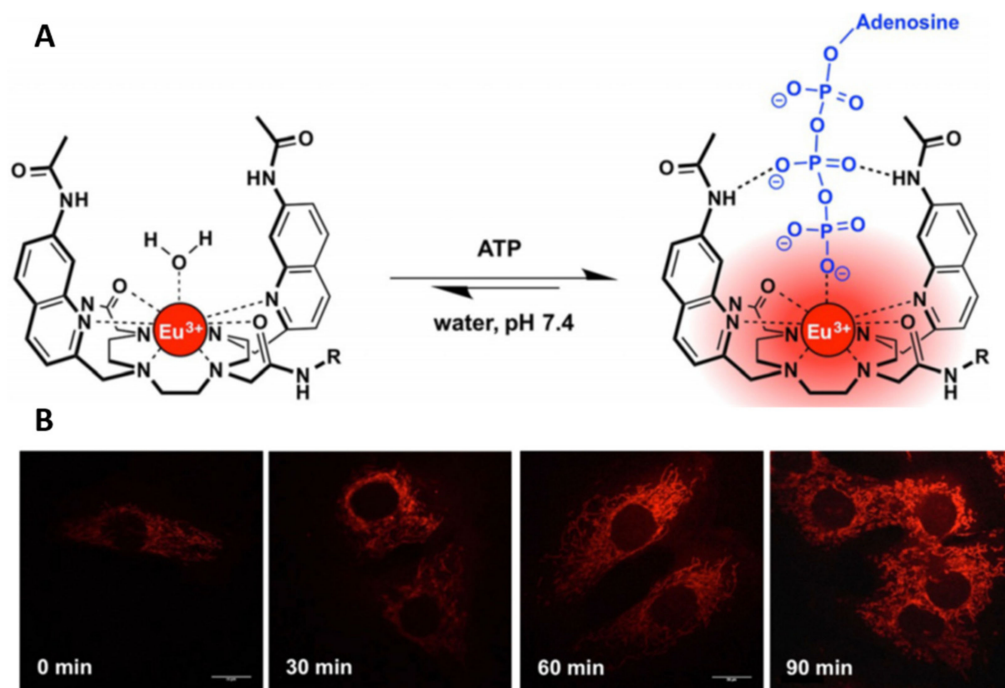**Figure 8.** Structures of Ir(III) complexes with organelle localisation highlighted in parenthesis.



**Figure 9.** An Eu(III) complex for mitochondrial ATP sensing. (**A**) The proposed binding mechanism between an Eu(III) complex and ATP to elicit a 'turn on' luminescent response. (**B**) NIH-3T3 cells treated with staurosporine (10 nM) and stained with an Eu(III) complex (50 μM, $\lambda_{exc}$ 355 nm, and $\lambda_{em}$ 605–720 nm), demonstrating real-time monitoring of ATP levels in mitochondria. Images adapted with permission [268]. Copyright 2018 Wiley-VCH.

The tracking of important biological molecules in live cells has also been achieved using metal ion complexes. Gillam and co-workers recently reported several neutral Re(I) complexes conjugated to sugar moieties (such as **ReMannose**, Figure 10) and tracked

their biodistribution in H9c2 cells using confocal microscopy [270]. Interestingly, it was found that biodistribution was not directed by the sugar moiety and rather the larger Re(I) complex. Conversely, Ir(III) complex **4**, which contains a glucose moiety tethered by a polar TEG chain, exhibited cellular uptake through GLUT transporters in HeLa cells [271], suggesting that the increased spacer provided by the water soluble linker played a significant role in the uptake mechanism. Recent work by Day et al. has conjugated a signalling peptide (PAAKRVKLD) to an Ir(III) complex to drive nucleus uptake. This imaging agent (**Ir-CMYC**) demonstrated co-staining with commercially nuclear stain Hoechst 33342 in fibroblast cells, exhibited near-IR emission, and was non-toxic [272]. However, conjugation with the metabolite of interest is not always the method used to track intracellular processes. For instance, Gill and co-workers reported a dinuclear Ru(II) dimer (**5**), which interacts with DNA to provide an environment-dependent emission in both prokaryotic and eukaryotic cells. This probe does not contain any specific directing motif yet still exhibits good selectivity to DNA [273].
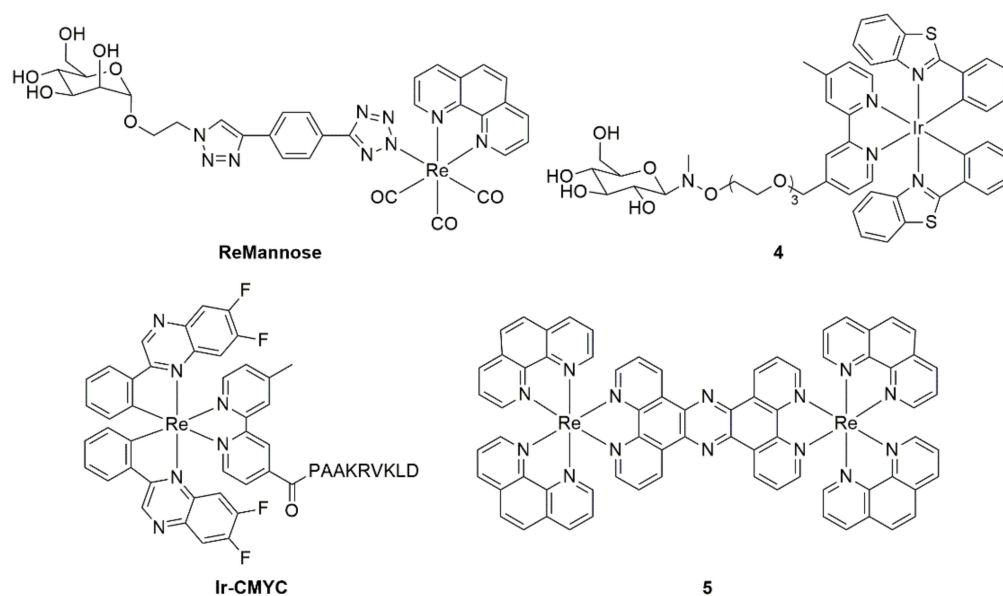


**Figure 10.** Structures of sugar conjugated metal ion complexes (ReMannose and **4**), nucleus imaging agent (Ir-CMYC), and DNA sensor (**5**).

### 4.4. Organic Fluorophores

Organic fluorophores enjoy a privileged place as the most prominent class of compounds for fluorescence imaging. Owing to their ready accessibility, small size, wide variety, and excellent emissive properties, organic fluorophores are frequently used for imaging cellular components, visualising cellular processes and tagging larger molecules (including antibodies and drugs) for insights into their cellular activity. The advantages and applications of organic fluorophores have been thoroughly covered in many excellent reviews [274–278], and their commercial availability renders their use as "plug and play" for cell biologists. Some common examples of commercially available fluorescent dyes include **Nile Red**, **MitoTracker™**, and **LysoTracker™**, for the staining of specific cellular organelles (see Figure 11), while the **Alexa Fluor** series of compounds are the most used tags for bioconjugation applications owing to their wide variety and established attachment chemistry. Structurally, these compounds are strikingly distinct and cover a range of different fluorophore classes; however, key functional groups are what typically drive cellular location for the organelle stains. For example, a diethylaniline is often used for lipid uptake (**Nile Red**), an overall positive charge typically leads to mitochondrial localisation (**MitoTracker™ Red**), and tertiary amines which become protonated in acidic environments are often employed for lysosomal uptake. In the case of fluorescent tags, the

key functional group facilitates the actual linkage between the fluorophore and the target of choice. In the case of the Alexa Fluor series depicted in Figure 11, this is achieved using carboxylate groups, which enable the formation of amide bonds.
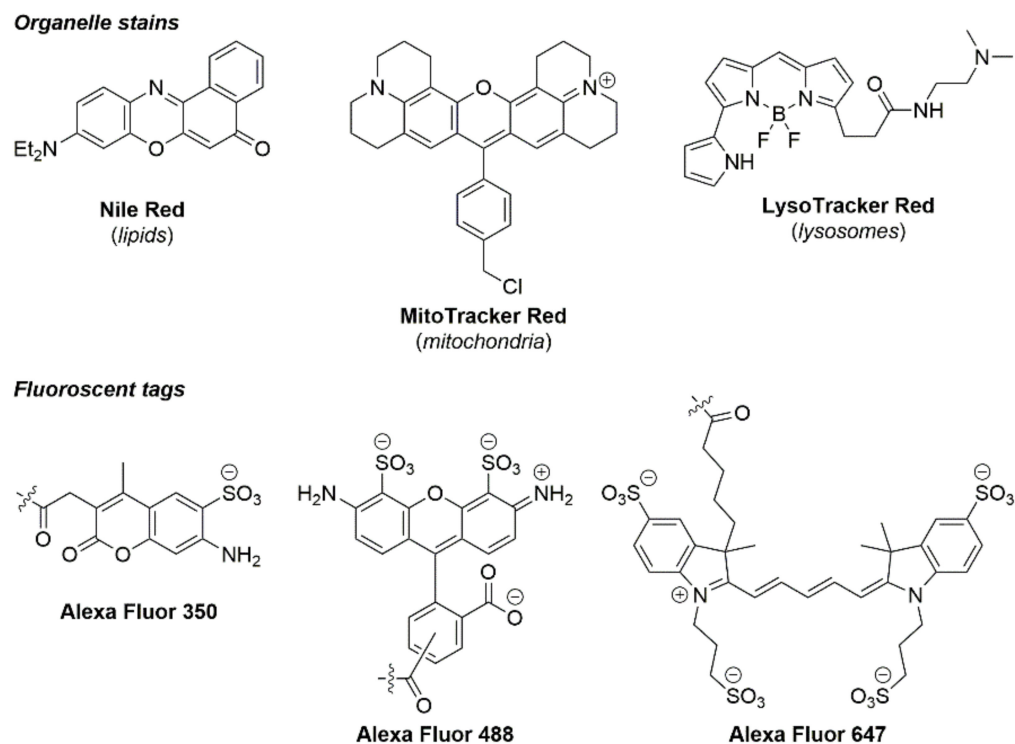


**Figure 11.** Commercially available fluorophores for organelle staining (**top**, target organelle in parenthesis) and bioconjugation (**below**).

The chemistry of organic fluorophores has been well investigated and new classes continue to be reported in the literature. Design considerations to improve the internal charge transfer (ICT), quantum yield, lifetime, and cell viability are commonly considered by chemists synthesising novel probes. A major advantage of small organic fluorophores is their capacity to be attached to larger molecules for tagging purposes (for example **Alexa Fluor™ 350**, **488**, and **647**). However, organic fluorophores often suffer from short lifetimes, photobleaching, cell toxicity, and poor solubility in aqueous environments. Nonetheless, organic fluorophores remain an indispensable tool for fluorescence microscopists for a range of applications.

The most common use of organic fluorophores in cellular imaging has traditionally been tagging of larger biomolecules, such as antibodies, peptides, or therapeutics, to investigate the mode of action studies [279] and cell function [277]. The addition of a bulky imaging agent tethered to a molecule of interest inherently casts doubt on whether its endogenous activity will be impacted. The fact that organic fluorophores are normally low molecular weight compounds is a prime reason for their monopoly for tagging applications.

The second most common use of organic fluorophores is to visualise subcellular structures. There are many commercially available dyes which are organelle-specific and are frequently used in co-localisation experiments to validate novel probes for this purpose, which may offer advantageous handling, photophysical, or toxicity properties. For example, a tetrazine-functionalised cyanine probe (**6**, Figure 12) has recently been used to react with cyclooctyne-labelled peptides to image actin filaments in Cos7 cells, using super resolution microscopy [280]. Lipid droplets (LDs) have garnered intense interest in the past few years as dynamic organelles essential to a wide variety of cellular processes. Imaging agents that selectively stain LDs are in high demand, such as the coumarin C-1, reported by Jana and co-workers, which was visualised in hepatoma cells at 200 nM, and confirmed using

differential interference contrast (DIC) illumination [281]. An excellent example of how structural changes significantly impact subcellular localisation was illustrated by Collot et al., who reported three squaraine compounds, each with different structural motifs, ultimately leading to distinct staining patterns in HeLa cells [282].



**Figure 12.** The structure of cyanine **6** and a micrograph demonstrating actin imaging in Cos7 cells after cyclisation with a small peptide. Scale bar = 5 μm. Reproduced with permission [280]. Copyright 2018 American Chemical Society.

Organic fluorophores are also ideally suited to monitor important cellular processes, owing to their wide ranging and accessible chemistries, which allow the synthesis of chemosensors designed for specific applications. The function of acetylcholinesterase (AChE) is critical for the conversion of acetylcholine to choline and acetate; a vital component of the nervous system. Recently, two near-IR emitting cyanine probes were developed, which were conjugated to huprine derivatives to enable AChE binding. **HupNIR2** (Figure 13) demonstrated excellent binding efficiency to AChE (IC50 = 31 ± 1.5 nM) and was visualised using fluorescence microscopy in a range of different cell types [283]. Another example of important cellular functions being monitored using fluorescence microscopy was described by Holmila et al., who reported coumarin compound **DCP-NEt₂C**, which was capable of capturing protein sulfenylation events, through reactivity with its 2,4-dioxocyclohexyl group, within the mitochondria of A549 cells, using confocal microscopy [284].
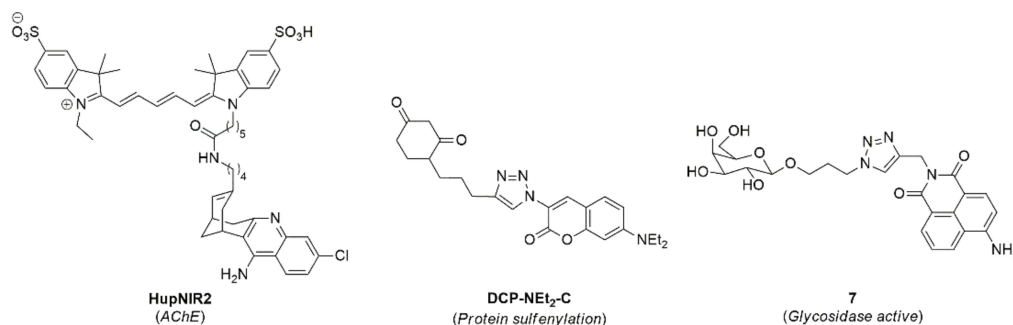


**Figure 13.** Organic fluorophores used for fluorescence imaging applications (shown in parentheses).

The ability of small organic fluorophores to act as drug-masks allows for the visualisation of drug delivery in real-time. For example, the Gunnlaugsson lab have reported a variety of chemosensors based on the 1,8-naphthalimide scaffold, including glycosylated derivatives (such as **7**) for the visualisation of glycosidase activity, as demonstrated in cancerous cell lines [285]. These probes were designed such that cellular uptake was only

permitted after the glycosidase enzyme cleaved the glycan unit from the imaging agent. Organic fluorophores have also found use as effective therapeutic agents harnessing their absorptive properties to give rise to photo-dynamic therapy. For example, a cisplatin-BODIPY conjugate was recently reported which was found to initiate ROS upon irradiation with near-IR light to invoke a cytotoxic response to A549 and HeLa cancer cells [286]. This conjugate was found to localise within the mitochondria of cells, which is the major cite of ROS production. The use of organic fluorophores in theranostics and photo-dynamic therapies has been well covered in the literature and the reader is directed to some excellent reviews on these topics [287,288].

## 5. Conclusions

This review has briefly outlined the three fundamental factors that need to be considered when designing fluorescence microscopy experiments. The most financially expensive consideration is what hardware is available and whether the parameters of this instrumentation will be suitable for the desired result. Careful design of an appropriate biological model which is amenable to fluorescence microscopy is required. Finally, the most suitable imaging agent to provide the fluorescent signal needs to be selected, with an ever-growing range of commercially available and literature-reported examples on offer. These three considerations are not mutually exclusive, with each factor impacting on the other two and ultimately driven by the intended outcome of the experimental data required. Consequently, an understanding of all aspects of hardware, imaging compounds, and in vitro or in vivo models is important when designing fluorescence microscopy experiments. As highlighted by numerous examples here, confocal microscopy dominates as the fluorescence microscopy hardware setup of choice. This is likely due to accessible cost and availability of these microscopes and the broad applicability to a range of imaging probes and biological models. Greater uptake and more widespread use of the advanced imaging hardware discussed in this review is likely to accelerate in the near future, as biologists look to harness the power of these instruments to gain a deeper understanding of cellular mechanisms and biology. We believe that this review will be helpful for those not fully versed across fluorescence microscopy to steer them towards experimental conditions and parameters which will aid in generating high quality and informative images for their intended applications.

## References

1. Renz, M. Fluorescence microscopy—A historical and technical perspective. *Cytom. Part A* **2013**, *83*, 767–779. [CrossRef] [PubMed]
2. Dunst, S.; Tomancak, P. Imaging flies by fluorescence microscopy: Principles, technologies, and applications. *Genetics* **2018**, *211*, 15–34. [CrossRef] [PubMed]
3. Chalfie, M.; Tu, Y.; Euskirchen, G.; Ward, W.W.; Prasher, D.C. Green fluorescent protein as a marker for gene expression. *Science* **1994**, *263*, 802–805. [CrossRef] [PubMed]

4.   Prasher, D.C.; Eckenrode, V.K.; Ward, W.W.; Prendergast, F.G.; Cormier, M.J. Primary structure of the aequorea victoria green-fluorescent protein. *Gene* **1992**, *111*, 229–233. [CrossRef]

5.   Marvin, M. Microscopy Apparatus. U.S. Patent 3,013,467, 19 December 1961.

6.   Minsky, M. Memoir on inventing the confocal scanning microscope. *Scanning* **1988**, *10*, 128–138. [CrossRef]

7.   Pawley, J. *Handbook of Biological Confocal Microscopy*; Springer Science & Business Media: Heidelberg, Germany, 2006; Volume 236.

8.   Murphy, D.B.; Michael, D. Two-photon excitation fluorescence microscopy. In *Fundamentals of Light Microscopy and Electronic Imaging*; John Wiley & Sons: Hoboken, NJ, USA, 2012; pp. 307–329.

9.   Ishikawa-Ankerhold, H.C.; Ankerhold, R.; Drummen, G.P.C. Advanced fluorescence microscopy techniques—Frap, flip, flap, fret and flim. *Molecules* **2012**, *17*, 4047–4132. [CrossRef]

10.  De Los Santos, C.; Chang, C.-W.; Mycek, M.-A.; Cardullo, R.A. Frap, flim, and fret: Detection and analysis of cellular dynamics on a molecular scale using fluorescence microscopy. *Mol. Reprod. Dev.* **2015**, *82*, 587–604. [CrossRef]

11.  Blacker, T.S.; Mann, Z.F.; Gale, J.E.; Ziegler, M.; Bain, A.J.; Szabadkai, G.; Duchen, M.R. Separating nadh and nadph fluorescence in live cells and tissues using flim. *Nat. Commun.* **2014**, *5*, 3936. [CrossRef]

12.  Sekar, R.B.; Periasamy, A. Fluorescence resonance energy transfer (fret) microscopy imaging of live cell protein localizations. *J. Cell Biol.* **2003**, *160*, 629–633. [CrossRef]

13.  Margineanu, A.; Chan, J.J.; Kelly, D.J.; Warren, S.C.; Flatters, D.; Kumar, S.; Katan, M.; Dunsby, C.W.; French, P.M.W. Screening for protein-protein interactions using förster resonance energy transfer (fret) and fluorescence lifetime imaging microscopy (flim). *Sci. Rep.* **2016**, *6*, 28186. [CrossRef]

14.  Blumenthal, D.; Goldstien, L.; Edidin, M.; Gheber, L.A. Universal approach to frap analysis of arbitrary bleaching patterns. *Sci. Rep.* **2015**, *5*, 11655. [CrossRef]

15.  Ji, N.; Magee, J.C.; Betzig, E. High-speed, low-photodamage nonlinear imaging using passive pulse splitters. *Nat. Methods* **2008**, *5*, 197–202. [CrossRef]

16.  Sakaguchi, H.; Ozaki, Y.; Ashida, T.; Matsubara, T.; Oishi, N.; Kihara, S.; Takahashi, J. Self-organized synchronous calcium transients in a cultured human neural network derived from cerebral organoids. *Stem Cell Rep.* **2019**, *13*, 458–473. [CrossRef]

17.  Au-Strobl, F.; Au-Klees, S.; Au-Stelzer, E.H.K. Light sheet-based fluorescence microscopy of living or fixed and stained tribolium castaneum embryos. *JoVE* **2017**, *122*, e55629.

18.  Ovečka, M.; von Wangenheim, D.; Tomančák, P.; Šamajová, O.; Komis, G.; Šamaj, J. Multiscale imaging of plant development by light-sheet fluorescence microscopy. *Nat. Plants* **2018**, *4*, 639–650. [CrossRef]

19.  Chakraborty, T.; Driscoll, M.K.; Jeffery, E.; Murphy, M.M.; Roudot, P.; Chang, B.-J.; Vora, S.; Wong, W.M.; Nielson, C.D.; Zhang, H.; et al. Light-sheet microscopy of cleared tissues with isotropic, subcellular resolution. *Nat. Methods* **2019**, *16*, 1109–1113. [CrossRef]

20.  Ueda, H.R.; Dodt, H.-U.; Osten, P.; Economo, M.N.; Chandrashekar, J.; Keller, P.J. Whole-brain profiling of cells and circuits in mammals by tissue clearing and light-sheet microscopy. *Neuron* **2020**, *106*, 369–387. [CrossRef]

21.  Chen, B.-C.; Legant, W.R.; Wang, K.; Shao, L.; Milkie, D.E.; Davidson, M.W.; Janetopoulos, C.; Wu, X.S.; Hammer, J.A.; Liu, Z.; et al. Lattice light-sheet microscopy: Imaging molecules to embryos at high spatiotemporal resolution. *Science* **2014**, *346*, 1257998. [CrossRef]

22.  Abbe, E. Contributions to the theory of the microscope and that microscopic perception. *Arch. Microsc. Anat.* **1873**, *9*, 413–468. [CrossRef]

23.  Perez, V.; Chang, B.-J.; Stelzer, E.H.K. Optimal 2d-sim reconstruction by two filtering steps with richardson-lucy deconvolution. *Sci. Rep.* **2016**, *6*, 37149. [CrossRef]

24.  Vicidomini, G.; Bianchini, P.; Diaspro, A. Sted super-resolved microscopy. *Nat. Methods* **2018**, *15*, 173–182. [CrossRef]

25.  Huff, J. The airyscan detector from zeiss: Confocal imaging with improved signal-to-noise ratio and super-resolution. *Nat. Methods* **2015**, *12*. [CrossRef]

26.  Wu, X.; Hammer, J.A. Zeiss airyscan: Optimizing usage for fast, gentle, super-resolution imaging. In *Confocal Microscopy: Methods and Protocols*; Brzostowski, J., Sohn, H., Eds.; Springer US: New York, NY, USA, 2021; pp. 111–130.

27.  Gustafsson, M.G.L. Surpassing the lateral resolution limit by a factor of two using structured illumination microscopy. *J. Microsc.* **2000**, *198*, 82–87. [CrossRef]

28.  Minner-Meinen, R.; Weber, J.-N.; Albrecht, A.; Matis, R.; Behnecke, M.; Tietge, C.; Frank, S.; Schulze, J.; Buschmann, H.; Walla, P.J.; et al. Split-halotag imaging assay for sophisticated microscopy of protein–protein interactions in planta. *Plant Commun.* **2021**, *2*, 100212. [CrossRef]

29.  Hinsdale, T.A.; Stallinga, S.; Rieger, B. High-speed multicolor structured illumination microscopy using a hexagonal single mode fiber array. *Biomed. Opt. Express* **2021**, *12*, 1181–1194. [CrossRef]

30.  Wu, Y.; Christensen, R.; Colón-Ramos, D.; Shroff, H. Advanced optical imaging techniques for neurodevelopment. *Curr. Opin. Neurobiol.* **2013**, *23*, 1090–1097. [CrossRef]

31.  Lin, R.; Kipreos, E.T.; Zhu, J.; Khang, C.H.; Kner, P. Subcellular three-dimensional imaging deep through multicellular thick samples by structured illumination microscopy and adaptive optics. *Nat. Commun.* **2021**, *12*, 3148. [CrossRef]

32.  Betzig, G.; Patterson, R.S.; OW, L.S. Olenych, js bonifacino, mw davidson, j. *Lippincott-Schwartz HF Hess Sci.* **2006**, *313*, 1642.

33.  Verma, A.; Verma, M.; Singh, A. Animal tissue culture principles and applications. *Anim. Biotechnol.* **2020**, 269–293. [CrossRef]

34.  Mirabelli, P.; Coppola, L.; Salvatore, M. Cancer cell lines are useful model systems for medical research. *Cancers* **2019**, *11*, 1098. [CrossRef]

35. Monici, M. Cell and tissue autofluorescence research and diagnostic applications. In *Biotechnology Annual Review*; Elsevier: Amsterdam, The Netherlands, 2005; Volume 11, pp. 227–256.

36. Wang, C.; Han, B.; Zhou, R.; Zhuang, X. Real-time imaging of translation on single mrna transcripts in live cells. *Cell* **2016**, *165*, 990–1001. [CrossRef] [PubMed]

37. Bandaria, J.N.; Qin, P.; Berk, V.; Chu, S.; Yildiz, A. Shelterin protects chromosome ends by compacting telomeric chromatin. *Cell* **2016**, *164*, 735–746. [CrossRef] [PubMed]

38. Carragher, N.O. Profiling distinct mechanisms of tumour invasion for drug discovery: Imaging adhesion, signalling and matrix turnover. *Clin. Exp. Metastasis* **2009**, *26*, 381–397. [CrossRef] [PubMed]

39. Johnson, I.R.D.; Parkinson-Lawrence, E.J.; Shandala, T.; Weigert, R.; Butler, L.M.; Brooks, D.A. Altered endosome biogenesis in prostate cancer has biomarker potential. *Mol. Cancer Res.* **2014**, *12*, 1851. [CrossRef] [PubMed]

40. Losavio, B.E.; Liang, Y.; Santamaría-Pang, A.; Kakadiaris, I.A.; Colbert, C.M.; Saggau, P. Live neuron morphology automatically reconstructed from multiphoton and confocal imaging data. *J. Neurophysiol.* **2008**, *100*, 2422–2429. [CrossRef] [PubMed]

41. Bodeen, W.J.; Marada, S.; Truong, A.; Ogden, S.K. A fixation method to preserve cultured cell cytonemes facilitates mechanistic interrogation of morphogen transport. *Development (Camb. Engl.)* **2017**, *144*, 3612–3624. [CrossRef] [PubMed]

42. Bhat, S.; Ljubojevic, N.; Zhu, S.; Fukuda, M.; Echard, A.; Zurzolo, C. Rab35 and its effectors promote formation of tunneling nanotubes in neuronal cells. *Sci. Rep.* **2020**, *10*, 16803. [CrossRef]

43. Zani, B.G.; Indolfi, L.; Edelman, E.R. Tubular bridges for bronchial epithelial cell migration and communication. *PLoS ONE* **2010**, *5*, e8930. [CrossRef]

44. Shabbir, A.; Cox, A.; Rodriguez-Menocal, L.; Salgado, M.; Van Badiavas, E. Mesenchymal stem cell exosomes induce proliferation and migration of normal and chronic wound fibroblasts, and enhance angiogenesis in vitro. *Stem Cells Dev.* **2015**, *24*, 1635–1647. [CrossRef]

45. Sigal, Y.M.; Zhou, R.; Zhuang, X. Visualizing and discovering cellular structures with super-resolution microscopy. *Science* **2018**, *361*, 880–887. [CrossRef]

46. Valm, A.M.; Cohen, S.; Legant, W.R.; Melunis, J.; Hershberg, U.; Wait, E.; Cohen, A.R.; Davidson, M.W.; Betzig, E.; Lippincott-Schwartz, J. Applying systems-level spectral imaging and analysis to reveal the organelle interactome. *Nature* **2017**, *546*, 162–167. [CrossRef]

47. Jensen, E.C. Overview of live-cell imaging: Requirements and methods used. *Anat. Rec.* **2013**, *296*, 1–8. [CrossRef]

48. Ettinger, A.; Wittmann, T. Chapter 5-fluorescence live cell imaging. In *Methods in Cell Biology*; Waters, J.C., Wittman, T., Eds.; Academic Press: Cambridge, MA, USA, 2014; Volume 123, pp. 77–94.

49. Bogdanov, A.M.; Kudryavtseva, E.I.; Lukyanov, K.A. Anti-fading media for live cell gfp imaging. *PLoS ONE* **2012**, *7*, e53004. [CrossRef]

50. Sasmal, M.; Bhowmick, R.; Musha Islam, A.S.; Bhuiya, S.; Das, S.; Ali, M. Domain-specific association of a phenanthrene–pyrene-based synthetic fluorescent probe with bovine serum albumin: Spectroscopic and molecular docking analysis. *ACS Omega* **2018**, *3*, 6293–6304. [CrossRef]

51. Lazniewska, J.; Agostino, M.; Hickey, S.M.; Parkinson-Lawrence, E.; Stagni, S.; Massi, M.; Brooks, D.A.; Plush, S.E. Spectroscopic and molecular docking study of the interaction between neutral re(i) tetrazolate complexes and bovine serum albumin. *Chem. –A Eur. J.* **2021**, *27*, 11406–11417. [CrossRef]

52. Gopalakrishnan, J. The emergence of stem cell-based brain organoids: Trends and challenges. *BioEssays* **2019**, *41*, 1900011. [CrossRef]

53. Rosenbluth, J.M.; Schackmann, R.C.J.; Gray, G.K.; Selfors, L.M.; Li, C.M.-C.; Boedicker, M.; Kuiken, H.J.; Richardson, A.; Brock, J.; Garber, J.; et al. Organoid cultures from normal and cancer-prone human breast tissues preserve complex epithelial lineages. *Nat. Commun.* **2020**, *11*, 1711. [CrossRef]

54. Drost, J.; Karthaus, W.R.; Gao, D.; Driehuis, E.; Sawyers, C.L.; Chen, Y.; Clevers, H. Organoid culture systems for prostate epithelial and cancer tissue. *Nat. Protoc.* **2016**, *11*, 347–358. [CrossRef]

55. Jensen, C.; Teng, Y. Is it time to start transitioning from 2d to 3d cell culture? *Front. Mol. Biosci.* **2020**, *7*, 33. [CrossRef]

56. Kim, M.; Mun, H.; Sung, C.O.; Cho, E.J.; Jeon, H.-J.; Chun, S.-M.; Jung, D.J.; Shin, T.H.; Jeong, G.S.; Kim, D.K.; et al. Patient-derived lung cancer organoids as in vitro cancer models for therapeutic screening. *Nat. Commun.* **2019**, *10*, 3991. [CrossRef]

57. Loong, H.H.F.; Wong, A.M.; Chan, D.T.M.; Cheung, M.S.H.; Chow, C.; Ding, X.; Chan, A.K.Y.; Johnston, P.A.; Lau, J.Y.W.; Poon, W.S.; et al. Patient-derived tumor organoid predicts drugs response in glioblastoma: A step forward in personalized cancer therapy? *J. Clin. Neurosci.* **2020**, *78*, 400–402. [CrossRef]

58. Lee, S.Y.; Ju, M.K.; Jeon, H.M.; Jeong, E.K.; Lee, Y.J.; Kim, C.H.; Park, H.G.; Han, S.I.; Kang, H.S. Regulation of tumor progression by programmed necrosis. *Oxidative Med. Cell. Longev.* **2018**, *2018*, 3537471. [CrossRef]

59. Pontes Soares, C.; Midlej, V.; de Oliveira, M.E.; Benchimol, M.; Costa, M.L.; Mermelstein, C. 2d and 3d-organized cardiac cells shows differences in cellular morphology, adhesion junctions, presence of myofibrils and protein expression. *PLoS ONE* **2012**, *7*, e38147.

60. Badder, L.M.; Hollins, A.J.; Herpers, B.; Yan, K.; Ewan, K.B.; Thomas, M.; Shone, J.R.; Badder, D.A.; Naven, M.; Ashelford, K.E.; et al. 3d imaging of colorectal cancer organoids identifies responses to tankyrase inhibitors. *PLoS ONE* **2020**, *15*, e0235319. [CrossRef] [PubMed]

61. Bowers, H.J.; Fannin, E.E.; Thomas, A.; Weis, J.A. Characterization of multicellular breast tumor spheroids using image data-driven biophysical mathematical modeling. *Sci. Rep.* **2020**, *10*, 11583. [CrossRef] [PubMed]

62. Hof, L.; Moreth, T.; Koch, M.; Liebisch, T.; Kurtz, M.; Tarnick, J.; Lissek, S.M.; Verstegen, M.M.A.; van der Laan, L.J.W.; Huch, M.; et al. Long-term live imaging and multiscale analysis identify heterogeneity and core principles of epithelial organoid morphogenesis. *BMC Biol.* **2021**, *19*, 37. [CrossRef]

63. Ritter, A.; Roth, S.; Kreis, N.N.; Friemel, A.; Hoock, S.C.; Steglich Souto, A.; Eichbaum, C.; Neuhoff, A.; Chen, Q.; Solbach, C.; et al. Primary cilia in trophoblastic cells: Potential involvement in preeclampsia. *Hypertension (Dallas Tex.: 1979)* **2020**, *76*, 1491–1505. [CrossRef]

64. Al-Ghadban, S.; Pursell, I.A.; Diaz, Z.T.; Herbst, K.L.; Bunnell, B.A. 3d spheroids derived from human lipedema ascs demonstrated similar adipogenic differentiation potential and ecm remodeling to non-lipedema ascs in vitro. *Int. J. Mol. Sci.* **2020**, *21*, 8350. [CrossRef]

65. Boyle, M.A.; Sequeira, D.J.; McNeill, E.P.; Criss, Z.K., 2nd; Shroyer, N.F.; Speer, A.L. In vivo transplantation of human intestinal organoids enhances select tight junction gene expression. *J. Surg. Res.* **2021**, *259*, 500–508. [CrossRef]

66. Park, M.; Kwon, J.; Shin, H.J.; Moon, S.M.; Kim, S.B.; Shin, U.S.; Han, Y.H.; Kim, Y. Butyrate enhances the efficacy of radiotherapy via foxo3a in colorectal cancer patient-derived organoids. *Int. J. Oncol.* **2020**, *57*, 1307–1318. [CrossRef]

67. Higa, K.; Higuchi, J.; Kimoto, R.; Miyashita, H.; Shimazaki, J.; Tsubota, K.; Shimmura, S. Human corneal limbal organoids maintaining limbal stem cell niche function. *Stem Cell Res.* **2020**, *49*, 102012. [CrossRef]

68. Johnsen, S.; Widder, E.A. The physical basis of transparency in biological tissue: Ultrastructure and the minimization of light scattering. *J. Theor. Biol.* **1999**, *199*, 181–198. [CrossRef]

69. Steelman, Z.A.; Eldridge, W.J.; Weintraub, J.B.; Wax, A. Is the nuclear refractive index lower than cytoplasm? Validation of phase measurements and implications for light scattering technologies. *J. Biophotonics* **2017**, *10*, 1714–1722. [CrossRef]

70. Costa, E.C.; Silva, D.N.; Moreira, A.F.; Correia, I.J. Optical clearing methods: An overview of the techniques used for the imaging of 3d spheroids. *Biotechnol. Bioeng.* **2019**, *116*, 2742–2763. [CrossRef]

71. Susaki, E.A.; Tainaka, K.; Perrin, D.; Kishino, F.; Tawara, T.; Watanabe, T.M.; Yokoyama, C.; Onoe, H.; Eguchi, M.; Yamaguchi, S.; et al. Whole-brain imaging with single-cell resolution using chemical cocktails and computational analysis. *Cell* **2014**, *157*, 726–739. [CrossRef]

72. Ertürk, A.; Becker, K.; Jährling, N.; Mauch, C.P.; Hojer, C.D.; Egen, J.G.; Hellal, F.; Bradke, F.; Sheng, M.; Dodt, H.-U. Three-dimensional imaging of solvent-cleared organs using 3disco. *Nat. Protoc.* **2012**, *7*, 1983–1995. [CrossRef]

73. Nürnberg, E.; Vitacolonna, M.; Klicks, J.; von Molitor, E.; Cesetti, T.; Keller, F.; Bruch, R.; Ertongur-Fauth, T.; Riedel, K.; Scholz, P.; et al. Routine optical clearing of 3d-cell cultures: Simplicity forward. *Front. Mol. Biosci.* **2020**, *7*, 20. [CrossRef]

74. Van Ineveld, R.L.; Ariese, H.C.R.; Wehrens, E.J.; Dekkers, J.F.; Rios, A.C. Single-cell resolution three-dimensional imaging of intact organoids. *J. Vis. Exp.* **2020**, *160*, e60709. [CrossRef]

75. Held, M.; Santeramo, I.; Wilm, B.; Murray, P.; Lévy, R. Ex vivo live cell tracking in kidney organoids using light sheet fluorescence microscopy. *PLoS ONE* **2018**, *13*, e0199918. [CrossRef]

76. O'Donnell, N.; Dmitriev, R.I. Three-dimensional tissue models and available probes for multi-parametric live cell microscopy: A brief overview. *Multi-Parametr. Live Cell Microsc. 3D Tissue Models* **2017**, *1035*, 49–67.

77. Theocharis, A.D.; Skandalis, S.S.; Gialeli, C.; Karamanos, N.K. Extracellular matrix structure. *Adv. Drug Deliv. Rev.* **2016**, *97*, 4–27. [CrossRef]

78. Mahajan, U.M.; Langhoff, E.; Goni, E.; Costello, E.; Greenhalf, W.; Halloran, C.; Ormanns, S.; Kruger, S.; Boeck, S.; Ribback, S.; et al. Immune cell and stromal signature associated with progression-free survival of patients with resected pancreatic ductal adenocarcinoma. *Gastroenterology* **2018**, *155*, 1625–1639.e1622. [CrossRef]

79. Wang, X.; Dong, B.; Zhang, K.; Ji, Z.; Cheng, C.; Zhao, H.; Sheng, Y.; Li, X.; Fan, L.; Xue, W.; et al. E-cadherin bridges cell polarity and spindle orientation to ensure prostate epithelial integrity and prevent carcinogenesis in vivo. *PLOS Genet.* **2018**, *14*, e1007609. [CrossRef]

80. Bass, B.P.; Engel, K.B.; Greytak, S.R.; Moore, H.M. A review of preanalytical factors affecting molecular, protein, and morphological analysis of formalin-fixed, paraffin-embedded (ffpe) tissue: How well do you know your ffpe specimen? *Arch. Pathol. Lab. Med.* **2014**, *138*, 1520–1530. [CrossRef]

81. Fujimoto, D.; Akiba, K.-Y.; Nakamura, N. Isolation and characterization of a fluorescent material in bovine achilles tendon collagen. *Biochem. Biophys. Res. Commun.* **1977**, *76*, 1124–1129. [CrossRef]

82. Blomfield, J.; Farrar, J.F. The fluorescent properties of maturing arterial elastin. *Cardiovasc. Res.* **1969**, *3*, 161–170. [CrossRef]

83. Davis, A.S.; Richter, A.; Becker, S.; Moyer, J.E.; Sandouk, A.; Skinner, J.; Taubenberger, J.K. Characterizing and diminishing autofluorescence in formalin-fixed paraffin-embedded human respiratory tissue. *J. Histochem. Cytochem.* **2014**, *62*, 405–423. [CrossRef]

84. Carriel, V.; Campos, F.; Aneiros-Fernández, J.; Kiernan, J.A. Tissue fixation and processing for the histological identification of lipids. In *Histochemistry of Single Molecules*; Springer: Berlin/Heidelberg, Germany, 2017; pp. 197–206.

85. Scalia, C.R.; Boi, G.; Bolognesi, M.M.; Riva, L.; Manzoni, M.; DeSmedt, L.; Bosisio, F.M.; Ronchi, S.; Leone, B.E.; Cattoretti, G. Antigen masking during fixation and embedding, dissected. *J. Histochem. Cytochem.* **2016**, *65*, 5–20. [CrossRef]

86.  Gao, X.H.; Li, J.; Gong, H.F.; Yu, G.Y.; Liu, P.; Hao, L.Q.; Liu, L.J.; Bai, C.G.; Zhang, W. Comparison of fresh frozen tissue with formalin-fixed paraffin-embedded tissue for mutation analysis using a multi-gene panel in patients with colorectal cancer. *Front. Oncol.* **2020**, *10*, 310. [CrossRef] [PubMed]

87.  Jensen, E. Technical review: In situ hybridization. *Anat. Rec.* **2014**, *297*, 1349–1353. [CrossRef] [PubMed]

88.  Chatterjee, S. Artefacts in histopathology. *J. Oral Maxillofac. Pathol.* **2014**, *18*, S111–S116. [CrossRef] [PubMed]

89.  Shi, S.-R.; Liu, C.; Pootrakul, L.; Tang, L.; Young, A.; Chen, R.; Cote, R.J.; Taylor, C.R. Evaluation of the value of frozen tissue section used as "gold standard" for immunohistochemistry. *Am. J. Clin. Pathol.* **2008**, *129*, 358–366. [CrossRef] [PubMed]

90.  Gaffney, E.F.; Riegman, P.H.; Grizzle, W.E.; Watson, P.H. Factors that drive the increasing use of ffpe tissue in basic and translational cancer research. *Biotech. Histochem.* **2018**, *93*, 373–386. [CrossRef] [PubMed]

91.  Mulligan, S.J.; MacVicar, B.A. Calcium transients in astrocyte endfeet cause cerebrovascular constrictions. *Nature* **2004**, *431*, 195–199. [CrossRef]

92.  Takano, T.; Tian, G.-F.; Peng, W.; Lou, N.; Libionka, W.; Han, X.; Nedergaard, M. Astrocyte-mediated control of cerebral blood flow. *Nat. Neurosci.* **2006**, *9*, 260–267. [CrossRef]

93.  Chen, Z.; Ross, J.L.; Hambardzumyan, D. Intravital 2-photon imaging reveals distinct morphology and infiltrative properties of glioblastoma-associated macrophages. *Proc. Natl. Acad. Sci. USA* **2019**, *116*, 14254–14259. [CrossRef]

94.  Lau, D.; Garçon, F.; Chandra, A.; Lechermann, L.M.; Aloj, L.; Chilvers, E.R.; Corrie, P.G.; Okkenhaug, K.; Gallagher, F.A. Intravital imaging of adoptive t-cell morphology, mobility and trafficking following immune checkpoint inhibition in a mouse melanoma model. *Front. Immunol.* **2020**, *11*, 11514. [CrossRef]

95.  Sugano, Y.; Siegfried, H.; Merkel, E.; Drummond, I.A. Novel transgenic lines to analyze renal glutathione redox potential in vivo. *Zebrafish* **2020**, *17*, 153–155. [CrossRef]

96.  Brighton, H.E.; Angus, S.P.; Bo, T.; Roques, J.; Tagliatela, A.C.; Darr, D.; Karagoz, K.; Sciaky, N.; Gatza, M.; Sharpless, N.E.; et al. New mechanisms of resistance to mek inhibitors in melanoma revealed by intravital imaging. *Cancer Res.* **2018**, *78*, 542–557. [CrossRef]

97.  Huang, Q.; Cohen, M.A.; Alsina, F.C.; Devlin, G.; Garrett, A.; McKey, J.; Havlik, P.; Rakhilin, N.; Wang, E.; Xiang, K.; et al. Intravital imaging of mouse embryos. *Science* **2020**, *368*, 181–186. [CrossRef]

98.  Dondossola, E.; Alexander, S.; Holzapfel, B.M.; Filippini, S.; Starbuck, M.W.; Hoffman, R.M.; Navone, N.; De-Juan-Pardo, E.M.; Logothetis, C.J.; Hutmacher, D.W.; et al. Intravital microscopy of osteolytic progression and therapy response of cancer lesions in the bone. *Sci. Transl. Med.* **2018**, *10*, 452. [CrossRef]

99.  Alieva, M.; Leidgens, V.; Riemenschneider, M.J.; Klein, C.A.; Hau, P.; van Rheenen, J. Intravital imaging of glioma border morphology reveals distinctive cellular dynamics and contribution to tumor cell invasion. *Sci. Rep.* **2019**, *9*, 2054. [CrossRef]

100. You, S.; Tu, H.; Chaney, E.J.; Sun, Y.; Zhao, Y.; Bower, A.J.; Liu, Y.-Z.; Marjanovic, M.; Sinha, S.; Pu, Y.; et al. Intravital imaging by simultaneous label-free autofluorescence-multiharmonic microscopy. *Nat. Commun.* **2018**, *9*, 2125. [CrossRef]

101. Seynhaeve, A.L.B.; Oostinga, D.; van Haperen, R.; Eilken, H.M.; Adams, S.; Adams, R.H.; ten Hagen, T.L.M. Spatiotemporal endothelial cell–pericyte association in tumors as shown by high resolution 4d intravital imaging. *Sci. Rep.* **2018**, *8*, 9596. [CrossRef]

102. Boulch, M.; Grandjean, C.L.; Cazaux, M.; Bousso, P. Tumor immunosurveillance and immunotherapies: A fresh look from intravital imaging. *Trends Immunol.* **2019**, *40*, 1022–1034. [CrossRef]

103. Nezu, A.; Morita, T.; Nagai, T.; Tanimura, A. Simultaneous monitoring of ca(2+) responses and salivary secretion in live animals reveals a threshold intracellular ca(2+) concentration for salivation. *Exp. Physiol.* **2019**, *104*, 61–69. [CrossRef]

104. Tvrdik, P.; Kearns, K.N.; Sharifi, K.A.; Sluzewski, M.F.; Acton, S.T.; Kalani, M.Y.S. Calcium imaging of microglial network activity in stroke. In *Microglia: Methods and Protocols*; Garaschuk, O., Verkhratsky, A., Eds.; Springer New York: New York, NY, USA, 2019; pp. 267–279.

105. Archambault, L.S.; Trzilova, D.; Gonia, S.; Gale, C.; Wheeler, R.T.; Gacser, A.; Hube, B. Intravital imaging reveals divergent cytokine and cellular immune responses to candida albicans and candida parapsilosis. *mBio* **2019**, *10*, e00266-19. [CrossRef]

106. Shandala, T.; Lim, C.; Sorvina, A.; Brooks, D.A. A drosophila model to image phagosome maturation. *Cells* **2013**, *2*, 188–201. [CrossRef]

107. Koyama, L.A.J.; Aranda-Díaz, A.; Su, Y.H.; Balachandra, S.; Martin, J.L.; Ludington, W.B.; Huang, K.C.; O'Brien, L.E. Bellymount enables longitudinal, intravital imaging of abdominal organs and the gut microbiota in adult drosophila. *PLoS Biol.* **2020**, *18*, e3000567. [CrossRef]

108. Sorvina, A.; Brooks, D.A.; Ng, Y.S.; Bader, C.A.; Weigert, R.; Shandala, T. Bacterial challenge initiates endosome-lysosome response in drosophila immune tissues. *IntraVital* **2013**, *2*, e23889. [CrossRef]

109. Asokan, N.; Daetwyler, S.; Bernas, S.N.; Schmied, C.; Vogler, S.; Lambert, K.; Wobus, M.; Wermke, M.; Kempermann, G.; Huisken, J.; et al. Long-term in vivo imaging reveals tumor-specific dissemination and captures host tumor interaction in zebrafish xenografts. *Sci. Rep.* **2020**, *10*, 13254. [CrossRef]

110. Revskoy, S.; Blair, M.E.; Powell, S.M.; Hausman, E.S.; Blackburn, J.S. In vivo imaging defines vascular interplay in the development of lymphocytic leukemia in zebrafish models. *bioRxiv* **2019**, 806562. [CrossRef]

111. Sedin, J.; Giraud, A.; Steiner, S.E.; Ahl, D.; Persson, A.E.G.; Melican, K.; Richter-Dahlfors, A.; Phillipson, M. High resolution intravital imaging of the renal immune response to injury and infection in mice. *Front. Immunol.* **2019**, *10*, 2744. [CrossRef]

112. Upadhaya, S.; Krichevsky, O.; Akhmetzyanova, I.; Sawai, C.M.; Fooksman, D.R.; Reizis, B. Intravital imaging reveals motility of adult hematopoietic stem cells in the bone marrow niche. *Cell Stem Cell* **2020**, *27*, 336–345.e334. [CrossRef]

113. Lai, C.W.; Chen, H.L.; Yen, C.C.; Wang, J.L.; Yang, S.H.; Chen, C.M. Using dual fluorescence reporting genes to establish an in vivo imaging model of orthotopic lung adenocarcinoma in mice. *Mol. Imaging Biol.* **2016**, *18*, 849–859. [CrossRef]

114. Ikeda, W.; Sasai, K.; Akagi, T. Imaging window device for subcutaneous implantation tumor. *Methods Mol. Biol. (Clifton N. J.)* **2018**, *1763*, 153–163.

115. Ryu, C.M.; Yu, H.Y.; Lee, H.Y.; Shin, J.H.; Lee, S.; Ju, H.; Paulson, B.; Lee, S.; Kim, S.; Lim, J.; et al. Longitudinal intravital imaging of transplanted mesenchymal stem cells elucidates their functional integration and therapeutic potency in an animal model of interstitial cystitis/bladder pain syndrome. *Theranostics* **2018**, *8*, 5610–5624. [CrossRef]

116. Fumagalli, A.; Bruens, L.; Scheele, C.; van Rheenen, J. Capturing stem cell behavior using intravital and live cell microscopy. *Cold Spring Harb. Perspect. Biol.* **2020**, *12*, a035949. [CrossRef] [PubMed]

117. Balan, M.; Trusohamn, M.; Ning, F.C.; Jacob, S.; Pietras, K.; Eriksson, U.; Berggren, P.-O.; Nyqvist, D. Noninvasive intravital high-resolution imaging of pancreatic neuroendocrine tumours. *Sci. Rep.* **2019**, *9*, 14636. [CrossRef] [PubMed]

118. Moon, J.; Kong, E.; Lee, J.; Jung, J.; Kim, E.; Park, S.B.; Kim, P. Intravital longitudinal imaging of hepatic lipid droplet accumulation in a murine model for nonalcoholic fatty liver disease. *Biomed. Opt. Express* **2020**, *11*, 5132–5146. [CrossRef] [PubMed]

119. Morikawa, T.; Tamaki, S.; Fujita, S.; Suematsu, M.; Takubo, K. Identification and local manipulation of bone marrow vasculature during intravital imaging. *Sci. Rep.* **2020**, *10*, 6422. [CrossRef]

120. Wu, J.; Lu, Z.; Jiang, D.; Guo, Y.; Qiao, H.; Zhang, Y.; Zhu, T.; Cai, Y.; Zhang, X.; Zhanghao, K.; et al. Iterative tomography with digital adaptive optics permits hour-long intravital observation of 3d subcellular dynamics at millisecond scale. *Cell* **2021**, *184*, 3318–3332.e3317. [CrossRef]

121. Hato, T.; Winfree, S.; Day, R.; Sandoval, R.M.; Molitoris, B.A.; Yoder, M.C.; Wiggins, R.C.; Zheng, Y.; Dunn, K.W.; Dagher, P.C. Two-photon intravital fluorescence lifetime imaging of the kidney reveals cell-type specific metabolic signatures. *J. Am. Soc. Nephrol. JASN* **2017**, *28*, 2420–2430. [CrossRef]

122. Rhodes, G.J. Surgical preparation of rats and mice for intravital microscopic imaging of abdominal organs. *Methods (San Diego Calif.)* **2017**, *128*, 129–138. [CrossRef]

123. Rompolas, P.; Deschene, E.R.; Zito, G.; Gonzalez, D.G.; Saotome, I.; Haberman, A.M.; Greco, V. Live imaging of stem cell and progeny behaviour in physiological hair-follicle regeneration. *Nature* **2012**, *487*, 496–499. [CrossRef]

124. Rompolas, P.; Mesa, K.R.; Greco, V. Spatial organization within a niche as a determinant of stem-cell fate. *Nature* **2013**, *502*, 513–518. [CrossRef]

125. Masedunskas, A.; Sramkova, M.; Parente, L.; Weigert, R. Intravital microscopy to image membrane trafficking in live rats. In *Cell Imaging Techniques: Methods and Protocols*; Taatjes, D.J., Roth, J., Eds.; Humana Press: Totowa, NJ, USA, 2013; pp. 153–167.

126. Shitara, A.; Bleck, C.K.E.; Weigert, R. Cdc42 controls secretory granules morphology in rodent salivary glands in vivo. *Commun. Integr. Biol.* **2020**, *13*, 22–26. [CrossRef]

127. Deane, J.A.; Abeynaike, L.D.; Norman, M.U.; Wee, J.L.; Kitching, A.R.; Kubes, P.; Hickey, M.J. Endogenous regulatory t cells adhere in inflamed dermal vessels via icam-1: Association with regulation of effector leukocyte adhesion. *J. Immunol. (Baltimore Md. 1950)* **2012**, *188*, 2179–2188. [CrossRef]

128. Liou, H.L.; Myers, J.T.; Barkauskas, D.S.; Huang, A.Y. Intravital imaging of the mouse popliteal lymph node. *J. Vis. Exp.* **2012**, *60*, e3720. [CrossRef]

129. Jang, W.H.; Park, A.; Wang, T.; Kim, C.J.; Chang, H.; Yang, B.-G.; Kim, M.J.; Myung, S.-J.; Im, S.-H.; Jang, M.H.; et al. Two-photon microscopy of paneth cells in the small intestine of live mice. *Sci. Rep.* **2018**, *8*, 14174. [CrossRef]

130. Jenne, C.N.; Wong, C.H.; Petri, B.; Kubes, P. The use of spinning-disk confocal microscopy for the intravital analysis of platelet dynamics in response to systemic and local inflammation. *PLoS ONE* **2011**, *6*, e25109. [CrossRef]

131. Alieva, M.; Ritsma, L.; Giedt, R.J.; Weissleder, R.; van Rheenen, J. Imaging windows for long-term intravital imaging: General overview and technical insights. *Intravital* **2014**, *3*, e29917. [CrossRef]

132. Prunier, C.; Chen, N.; Ritsma, L.; Vrisekoop, N. Procedures and applications of long-term intravital microscopy. *Methods (San Diego Calif.)* **2017**, *128*, 52–64. [CrossRef]

133. Rouffiac, V.; Ser-Le Roux, K.; Salomé-Desnoulez, S.; Leguerney, I.; Ginefri, J.C.; Sébrié, C.; Jourdain, L.; Lécluse, Y.; Laplace-Builhé, C. Multimodal imaging for tumour characterization from micro- to macroscopic level using a newly developed dorsal chamber designed for long-term follow-up. *J. Biophotonics* **2020**, *13*, e201900217.

134. Ritsma, L.; Steller, E.J.; Ellenbroek, S.I.; Kranenburg, O.; Borel Rinkes, I.H.; van Rheenen, J. Surgical implantation of an abdominal imaging window for intravital microscopy. *Nat. Protoc.* **2013**, *8*, 583–594. [CrossRef]

135. Lefrançais, E.; Ortiz-Muñoz, G.; Caudrillier, A.; Mallavia, B.; Liu, F.; Sayah, D.M.; Thornton, E.E.; Headley, M.B.; David, T.; Coughlin, S.R.; et al. The lung is a site of platelet biogenesis and a reservoir for haematopoietic progenitors. *Nature* **2017**, *544*, 105–109. [CrossRef]

136. Thanabalasuriar, A.; Neupane, A.S.; Wang, J.; Krummel, M.F.; Kubes, P. Inkt cell emigration out of the lung vasculature requires neutrophils and monocyte-derived dendritic cells in inflammation. *Cell Rep.* **2016**, *16*, 3260–3272. [CrossRef]

137. Seynhaeve, A.L.B.; Ten Hagen, T.L.M. Intravital microscopy of tumor-associated vasculature using advanced dorsal skinfold window chambers on transgenic fluorescent mice. *J. Vis. Exp.* **2018**, *131*, 55115. [CrossRef]

138. Kilarski, W.W.; Güç, E.; Swartz, M.A. Dorsal ear skin window for intravital imaging and functional analysis of lymphangiogenesis. *Methods Mol. Biol. (Clifton N. J.)* **2018**, *1846*, 261–277.

139. Haghayegh Jahromi, N.; Tardent, H.; Enzmann, G.; Deutsch, U.; Kawakami, N.; Bittner, S.; Vestweber, D.; Zipp, F.; Stein, J.V.; Engelhardt, B. A novel cervical spinal cord window preparation allows for two-photon imaging of t-cell interactions with the cervical spinal cord microvasculature during experimental autoimmune encephalomyelitis. *Front. Immunol.* **2017**, *8*, 406. [CrossRef] [PubMed]

140. Askoxylakis, V.; Badeaux, M.; Roberge, S.; Batista, A.; Kirkpatrick, N.; Snuderl, M.; Amoozgar, Z.; Seano, G.; Ferraro, G.B.; Chatterjee, S.; et al. A cerebellar window for intravital imaging of normal and disease states in mice. *Nat. Protoc.* **2017**, *12*, 2251–2262. [CrossRef] [PubMed]

141. Barretto, R.P.J.; Ko, T.H.; Jung, J.C.; Wang, T.J.; Capps, G.; Waters, A.C.; Ziv, Y.; Attardo, A.; Recht, L.; Schnitzer, M.J. Time-lapse imaging of disease progression in deep brain areas using fluorescence microendoscopy. *Nat. Med.* **2011**, *17*, 223–228. [CrossRef] [PubMed]

142. Zhang, H.; Vyas, K.; Yang, G.Z. Line scanning, fiber bundle fluorescence hilo endomicroscopy with confocal slit detection. *J. Biomed. Opt.* **2019**, *24*, 1–7. [CrossRef] [PubMed]

143. Paulson, B.; Kim, I.H.; Namgoong, J.M.; Kim, Y.G.; Lee, S.; Moon, Y.; Shin, D.M.; Choo, M.S.; Kim, J.K. Longitudinal micro-endoscopic monitoring of high-success intramucosal xenografts for mouse models of colorectal cancer. *Int. J. Med. Sci.* **2019**, *16*, 1453–1460. [CrossRef] [PubMed]

144. Bae, S.M.; Bae, D.-J.; Do, E.-J.; Oh, G.; Yoo, S.W.; Lee, G.-J.; Chae, J.S.; Yun, Y.; Kim, S.; Kim, K.H.; et al. Multi-spectral fluorescence imaging of colon dysplasia in vivo using a multi-spectral endoscopy system. *Transl. Oncol.* **2019**, *12*, 226–235. [CrossRef]

145. Boerwinkel, D.F.; Holz, J.A.; Hawkins, D.M.; Curvers, W.L.; Aalders, M.C.; Weusten, B.L.; Visser, M.; Meijer, S.L.; Bergman, J.J. Fluorescence spectroscopy incorporated in an optical biopsy system for the detection of early neoplasia in barrett's esophagus. *Dis. Esophagus Off. J. Int. Soc. Dis. Esophagus* **2015**, *28*, 345–351. [CrossRef]

146. Jun, E.J.; Song, H.Y.; Park, J.H.; Bae, Y.S.; Paulson, B.; Lee, S.; Cho, Y.C.; Tsauo, J.; Kim, M.T.; Kim, K.Y.; et al. In vivo fluorescence microendoscopic monitoring of stent-induced fibroblast cell proliferation in an esophageal mouse model. *J. Vasc. Interv. Radiol. JVIR* **2018**, *29*, 1756–1763. [CrossRef]

147. Trindade, J.R.M.; Figueiredo, V.R.; Pêgo-Fernandes, P.M.; Terra, R.M. Probe-based confocal laser endomicroscopy of the airways: Physiological and pathological characteristics of preneoplastic and neoplastic lesions. *J. Bras. Pneumol.* **2019**, *45*, e20180103. [CrossRef]

148. Lee, S.; Vinegoni, C.; Sebas, M.; Weissleder, R. Automated motion artifact removal for intravital microscopy, without a priori information. *Sci. Rep.* **2014**, *4*, 4507. [CrossRef]

149. Soulet, D.; Lamontagne-Proulx, J.; Aube, B.; Davalos, D. Multiphoton intravital microscopy in small animals: Motion artefact challenges and technical solutions. *J. Microsc.* **2020**, *278*, 3–17. [CrossRef]

150. Chatalic, K.L.S.; Kwekkeboom, D.J.; de Jong, M. Radiopeptides for imaging and therapy: A radiant future. *J. Nucl. Med.* **2015**, *56*, 1809. [CrossRef]

151. Wadas, T.J.; Wong, E.H.; Weisman, G.R.; Anderson, C.J. Coordinating radiometals of copper, gallium, indium, yttrium, and zirconium for pet and spect imaging of disease. *Chem. Rev.* **2010**, *110*, 2858–2902. [CrossRef]

152. Thakor, A.S.; Jokerst, J.V.; Ghanouni, P.; Campbell, J.L.; Mittra, E.; Gambhir, S.S. Clinically approved nanoparticle imaging agents. *J. Nucl. Med.* **2016**, *57*, 1833. [CrossRef]

153. Torchilin, V.P. Recent advances with liposomes as pharmaceutical carriers. *Nat. Rev. Drug Discov.* **2005**, *4*, 145–160. [CrossRef]

154. Gindy, M.E.; Prud'homme, R.K. Multifunctional nanoparticles for imaging, delivery and targeting in cancer therapy. *Expert Opin. Drug Deliv.* **2009**, *6*, 865–878. [CrossRef]

155. Forte, E.; Fiorenza, D.; Torino, E.; Costagliola di Polidoro, A.; Cavaliere, C.; Netti, P.A.; Salvatore, M.; Aiello, M. Radiolabeled pet/mri nanoparticles for tumor imaging. *J. Clin. Med.* **2020**, *9*, 89. [CrossRef]

156. Bouziotis, P.; Stellas, D.; Thomas, E.; Truillet, C.; Tsoukalas, C.; Lux, F.; Tsotakos, T.; Xanthopoulos, S.; Paravatou-Petsotas, M.; Gaitanis, A. 68ga-radiolabeled aguix nanoparticles as dual-modality imaging agents for pet/mri-guided radiation therapy. *Nanomedicine* **2017**, *12*, 1561–1574. [CrossRef]

157. Motiei, M.; Dreifuss, T.; Sadan, T.; Omer, N.; Blumenfeld-Katzir, T.; Fragogeorgi, E.; Loudos, G.; Popovtzer, R.; Ben-Eliezer, N. Trimodal nanoparticle contrast agent for ct, mri and spect imaging: Synthesis and characterization of radiolabeled core/shell iron oxide@ gold nanoparticles. *Chem. Lett.* **2019**, *48*, 291–294. [CrossRef]

158. Imlimthan, S.; Otaru, S.; Keinaänen, O.; Correia, A.; Lintinen, K.; Santos, H.A.; Airaksinen, A.J.; Kostiainen, M.A.; Sarparanta, M. Radiolabeled molecular imaging probes for the in vivo evaluation of cellulose nanocrystals for biomedical applications. *Biomacromolecules* **2018**, *20*, 674–683. [CrossRef]

159. Köker, T.; Tang, N.; Tian, C.; Zhang, W.; Wang, X.; Martel, R.; Pinaud, F. Cellular imaging by targeted assembly of hot-spot sers and photoacoustic nanoprobes using split-fluorescent protein scaffolds. *Nat. Commun.* **2018**, *9*, 607. [CrossRef]

160. Qian, X.M.; Nie, S.M. Single-molecule and single-nanoparticle sers: From fundamental mechanisms to biomedical applications. *Chem. Soc. Rev.* **2008**, *37*, 912–920. [CrossRef]

161. Chow, K.; Tyrrell, D.; Yang, M.; Abraham, L.; Anderson, G.; Mansfield, C. Scintigraphic assessment of deposition of radiolabeled fluticasone delivered from a nebulizer and metered dose inhaler in 10 healthy dogs. *J. Vet. Intern. Med.* **2017**, *31*, 1849–1857. [CrossRef]

162. Shimomura, O.; Johnson, F.H.; Saiga, Y. Extraction, purification and properties of aequorin, a bioluminescent protein from the luminous hydromedusan, aequorea. *J. Cell. Comp. Physiol.* **1962**, *59*, 223–239. [CrossRef]

163. Kremers, G.J.; Gilbert, S.G.; Cranfill, P.J.; Davidson, M.W.; Piston, D.W. Fluorescent proteins at a glance. *J. Cell Sci.* **2011**, *124*, 157–160. [CrossRef]

164. Chudakov, D.M.; Matz, M.V.; Lukyanov, S.; Lukyanov, K.A. Fluorescent proteins and their applications in imaging living cells and tissues. *Physiol. Rev.* **2010**, *90*, 1103–1163. [CrossRef]

165. Miyawaki, A.; Niino, Y. Molecular spies for bioimaging—Fluorescent protein-based probes. *Mol. Cell* **2015**, *58*, 632–643. [CrossRef]

166. Patterson, G.H.; Lippincott-Schwartz, J. A photoactivatable gfp for selective photolabeling of proteins and cells. *Science* **2002**, *297*, 1873. [CrossRef]

167. Ganini, D.; Leinisch, F.; Kumar, A.; Jiang, J.; Tokar, E.J.; Malone, C.C.; Petrovich, R.M.; Mason, R.P. Fluorescent proteins such as egfp lead to catalytic oxidative stress in cells. *Redox Biol.* **2017**, *12*, 462–468. [CrossRef]

168. Stadler, C.; Rexhepaj, E.; Singan, V.R.; Murphy, R.F.; Pepperkok, R.; Uhlén, M.; Simpson, J.C.; Lundberg, E. Immunofluorescence and fluorescent-protein tagging show high correlation for protein localization in mammalian cells. *Nat. Methods* **2013**, *10*, 315–323. [CrossRef]

169. Cranfill, P.J.; Sell, B.R.; Baird, M.A.; Allen, J.R.; Lavagnino, Z.; de Gruiter, H.M.; Kremers, G.J.; Davidson, M.W.; Ustione, A.; Piston, D.W. Quantitative assessment of fluorescent proteins. *Nat. Methods* **2016**, *13*, 557–562. [CrossRef]

170. Zacharias, D.A.; Violin, J.D.; Newton, A.C.; Tsien, R.Y. Partitioning of lipid-modified monomeric gfps into membrane microdomains of live cells. *Science* **2002**, *296*, 913–916. [CrossRef] [PubMed]

171. Snapp, E.L. Fluorescent proteins: A cell biologist's user guide. *Trends Cell Biol.* **2009**, *19*, 649–655. [CrossRef] [PubMed]

172. Wu, J.; Jaffrey, S.R. Imaging mrna trafficking in living cells using fluorogenic proteins. *Curr. Opin. Chem. Biol.* **2020**, *57*, 177–183. [CrossRef] [PubMed]

173. Shaner, N.C.; Steinbach, P.A.; Tsien, R.Y. A guide to choosing fluorescent proteins. *Nat. Methods* **2005**, *2*, 905–909. [CrossRef]

174. Megason, S.G.; Fraser, S.E. Imaging in systems biology. *Cell* **2007**, *130*, 784–795. [CrossRef]

175. Oliva Trejo, J.A.; Tanida, I.; Suzuki, C.; Kakuta, S.; Tada, N.; Uchiyama, Y. Characterization of starvation-induced autophagy in cerebellar purkinje cells of phluorin-mkate2-human lc3b transgenic mice. *Sci. Rep.* **2020**, *10*, 9643. [CrossRef]

176. Bozhanova, N.G.; Baranov, M.S.; Klementieva, N.V.; Sarkisyan, K.S.; Gavrikov, A.S.; Yampolsky, I.V.; Zagaynova, E.V.; Lukyanov, S.A.; Lukyanov, K.A.; Mishin, A.S. Protein labeling for live cell fluorescence microscopy with a highly photostable renewable signal. *Chem. Sci.* **2017**, *8*, 7138–7142. [CrossRef]

177. Wu, J.; Zaccara, S.; Khuperkar, D.; Kim, H.; Tanenbaum, M.E.; Jaffrey, S.R. Live imaging of mrna using rna-stabilized fluorogenic proteins. *Nat. Methods* **2019**, *16*, 862–865. [CrossRef]

178. Bertrand, E.; Chartrand, P.; Schaefer, M.; Shenoy, S.M.; Singer, R.H.; Long, R.M. Localization of ash1 mrna particles in living yeast. *Mol. Cell* **1998**, *2*, 437–445. [CrossRef]

179. Vera, M.; Tutucci, E.; Singer, R.H. Imaging single mrna molecules in mammalian cells using an optimized ms2-mcp system. In *Imaging Gene Expression*; Springer: Berlin/Heidelberg, Germany, 2019; pp. 3–20.

180. Tutucci, E.; Vera, M.; Biswas, J.; Garcia, J.; Parker, R.; Singer, R.H. An improved ms2 system for accurate reporting of the mrna life cycle. *Nat. Methods* **2018**, *15*, 81–89. [CrossRef]

181. Filonov, G.S.; Moon, J.D.; Svensen, N.; Jaffrey, S.R. Broccoli: Rapid selection of an rna mimic of green fluorescent protein by fluorescence-based selection and directed evolution. *J. Am. Chem. Soc.* **2014**, *136*, 16299–16308. [CrossRef]

182. Paige, J.S.; Wu, K.Y.; Jaffrey, S.R. Rna mimics of green fluorescent protein. *Science* **2011**, *333*, 642. [CrossRef]

183. Weissman, T.A.; Pan, Y.A. Brainbow: New resources and emerging biological applications for multicolor genetic labeling and analysis. *Genetics* **2015**, *199*, 293–306. [CrossRef]

184. Roo, J.J.d.; Vloemans, S.A.; Vrolijk, H.; Haas, E.F.d.; Staal, F.J. Development of an in vivo model to study clonal lineage relationships in hematopoietic cells using brainbow2.1/confetti mice. *Future Sci. OA* **2019**, *5*, FSO427. [CrossRef]

185. El-Nachef, D.; Shi, K.; Beussman, K.M.; Martinez, R.; Regier, M.C.; Everett, G.W.; Murry, C.E.; Stevens, K.R.; Young, J.E.; Sniadecki, N.J.; et al. A rainbow reporter tracks single cells and reveals heterogeneous cellular dynamics among pluripotent stem cells and their differentiated derivatives. *Stem Cell Rep.* **2020**, *15*, 226–241. [CrossRef]

186. Cook, Z.T.; Brockway, N.L.; Tobias, Z.J.C.; Pajarla, J.; Boardman, I.S.; Ippolito, H.; Nkoula, S.N.; Weissman, T.A. Combining near-infrared fluorescence with brainbow to visualize expression of specific genes within a multicolor context. *Mol. Biol. Cell* **2019**, *30*, 491–505. [CrossRef]

187. Specht, E.A.; Braselmann, E.; Palmer, A.E. A critical and comparative review of fluorescent tools for live-cell imaging. *Annu. Rev. Physiol.* **2017**, *79*, 93–117. [CrossRef]

188. Wei, L.; Chen, Z.; Shi, L.; Long, R.; Anzalone, A.V.; Zhang, L.; Hu, F.; Yuste, R.; Cornish, V.W.; Min, W. Super-multiplex vibrational imaging. *Nature* **2017**, *544*, 465–470. [CrossRef]

189. Shen, Y.; Wu, S.-Y.; Rancic, V.; Aggarwal, A.; Qian, Y.; Miyashita, S.-I.; Ballanyi, K.; Campbell, R.E.; Dong, M. Genetically encoded fluorescent indicators for imaging intracellular potassium ion concentration. *Commun. Biol.* **2019**, *2*, 18. [CrossRef]

190. Udensi, U.K.; Tchounwou, P.B. Potassium homeostasis, oxidative stress, and human disease. *Int. J. Clin. Exp. Physiol.* **2017**, *4*, 111–122.

191. Angres, B.; Steuer, H.; Weber, P.; Wagner, M.; Schneckenburger, H. A membrane-bound fret-based caspase sensor for detection of apoptosis using fluorescence lifetime and total internal reflection microscopy. *Cytom. Part A* **2009**, *75A*, 420–427. [CrossRef]

192. Savitsky, A.P.; Rusanov, A.L.; Zherdeva, V.V.; Gorodnicheva, T.V.; Khrenova, M.G.; Nemukhin, A.V. Flim-fret imaging of caspase-3 activity in live cells using pair of red fluorescent proteins. *Theranostics* **2012**, *2*, 215–226. [CrossRef]

193. Heim, R.; Tsien, R.Y. Engineering green fluorescent protein for improved brightness, longer wavelengths and fluorescence resonance energy transfer. *Curr. Biol.* **1996**, *6*, 178–182. [CrossRef]

194. Erismann-Ebner, K.; Marowsky, A.; Arand, M. In-vitro characterization of mcerulean3_mruby3 as a novel fret pair with favorable bleed-through characteristics. *Biosensors* **2019**, *9*, 33. [CrossRef]

195. George Abraham, B.; Sarkisyan, K.S.; Mishin, A.S.; Santala, V.; Tkachenko, N.V.; Karp, M. Fluorescent protein based fret pairs with improved dynamic range for fluorescence lifetime measurements. *PLoS ONE* **2015**, *10*, e0134436. [CrossRef]

196. Umrao, S.; Jain, V.; Anusha; Chakraborty, B.; Roy, R. Protein-induced fluorescence enhancement as aptamer sensing mechanism for thrombin detection. *Sens. Actuators B Chem.* **2018**, *267*, 294–301. [CrossRef]

197. Vanderklish, P.W.; Krushel, L.A.; Holst, B.H.; Gally, J.A.; Crossin, K.L.; Edelman, G.M. Marking synaptic activity in dendritic spines with a calpain substrate exhibiting fluorescence resonance energy transfer. *Proc. Natl. Acad. Sci. USA* **2000**, *97*, 2253. [CrossRef]

198. Stockholm, D.; Bartoli, M.; Sillon, G.; Bourg, N.; Davoust, J.; Richard, I. Imaging calpain protease activity by multiphoton fret in living mice. *J. Mol. Biol.* **2005**, *346*, 215–222. [CrossRef]

199. Mo, G.C.; Posner, C.; Rodriguez, E.A.; Sun, T.; Zhang, J. A rationally enhanced red fluorescent protein expands the utility of fret biosensors. *Nat. Commun.* **2020**, *11*, 1–9. [CrossRef]

200. Duwé, S.; Dedecker, P. Optimizing the fluorescent protein toolbox and its use. *Curr. Opin. Biotechnol.* **2019**, *58*, 183–191. [CrossRef]

201. Kleeman, B.; Olsson, A.; Newkold, T.; Kofron, M.; DeLay, M.; Hildeman, D.; Grimes, H.L. A guide to choosing fluorescent protein combinations for flow cytometric analysis based on spectral overlap. *Cytom. Part A* **2018**, *93*, 556–562. [CrossRef] [PubMed]

202. Richards, R.; Mason, D.; Kelly, R.; Lévy, R.; Bearon, R.; Sée, V. 4d imaging and analysis of multicellular tumour spheroid cell migration and invasion. *bioRxiv* **2019**, 443648. [CrossRef]

203. Shashkova, S.; Leake, M.C. Single-molecule fluorescence microscopy review: Shedding new light on old problems. *Biosci. Rep.* **2017**, *37*, BSR20170031. [CrossRef] [PubMed]

204. Johnson, N.; Glick, B.S. 4D microscopy of yeast. *J. Vis. Exp.* **2019**, *146*. [CrossRef]

205. Descloux, A.; Grußmayer, K.S.; Bostan, E.; Lukes, T.; Bouwens, A.; Sharipov, A.; Geissbuehler, S.; Mahul-Mellier, A.L.; Lashuel, H.A.; Leutenegger, M.; et al. Combined multi-plane phase retrieval and super-resolution optical fluctuation imaging for 4d cell microscopy. *Nat. Photonics* **2018**, *12*, 165–172. [CrossRef]

206. Politi, A.Z.; Cai, Y.; Walther, N.; Hossain, M.J.; Koch, B.; Wachsmuth, M.; Ellenberg, J. Quantitative mapping of fluorescently tagged cellular proteins using fcs-calibrated four-dimensional imaging. *Nat. Protoc.* **2018**, *13*, 1445–1464. [CrossRef]

207. Yong, K.-T.; Law, W.-C.; Hu, R.; Ye, L.; Liu, L.; Swihart, M.T.; Prasad, P.N. Nanotoxicity assessment of quantum dots: From cellular to primate studies. *Chem. Soc. Rev.* **2013**, *42*, 1236–1250. [CrossRef]

208. Han, X.; Xu, K.; Taratula, O.; Farsad, K. Applications of nanoparticles in biomedical imaging. *Nanoscale* **2019**, *11*, 799–819. [CrossRef]

209. Goreham, R.V.; Schroeder, K.L.; Holmes, A.; Bradley, S.J.; Nann, T. Demonstration of the lack of cytotoxicity of unmodified and folic acid modified graphene oxide quantum dots, and their application to fluorescence lifetime imaging of hacat cells. *Microchim. Acta* **2018**, *185*, 128. [CrossRef]

210. Mei, K.-C.; Rubio, N.; Costa, P.M.; Kafa, H.; Abbate, V.; Festy, F.; Bansal, S.S.; Hider, R.C.; Al-Jamal, K.T. Synthesis of double-clickable functionalised graphene oxide for biological applications. *Chem. Commun.* **2015**, *51*, 14981–14984. [CrossRef]

211. Jiang, D.; Chen, Y.; Li, N.; Li, W.; Wang, Z.; Zhu, J.; Zhang, H.; Liu, B.; Xu, S. Synthesis of luminescent graphene quantum dots with high quantum yield and their toxicity study. *PLoS ONE* **2016**, *10*, e0144906. [CrossRef]

212. Mitchell, B.; Bradley, S.J.; Thomas, N. Graphene quantum dots. *Part. Part. Syst. Charact.* **2014**, *31*, 415–428.

213. Shen, J.; Zhu, Y.; Yang, X.; Li, C. Graphene quantum dots: Emergent nanolights for bioimaging, sensors, catalysis and photovoltaic devices. *Chem. Commun.* **2012**, *48*, 3686–3699. [CrossRef]

214. Chung, S.; Revia, R.A.; Zhang, M. Graphene quantum dots and their applications in bioimaging, biosensing, and therapy. *Adv. Mater.* **2021**, *33*, 1904362. [CrossRef]

215. Sweetman, M.J.; Hickey, S.M.; Brooks, D.A.; Hayball, J.D.; Plush, S.E. A practical guide to prepare and synthetically modify graphene quantum dots. *Adv. Funct. Mater.* **2019**, *29*, 1808740–1808758. [CrossRef]

216. Georgakilas, V.; Otyepka, M.; Bourlinos, A.B.; Chandra, V.; Kim, N.; Kemp, K.C.; Hobza, P.; Zboril, R.; Kim, K.S. Functionalization of graphene: Covalent and non-covalent approaches, derivatives and applications. *Chem. Rev.* **2012**, *112*, 6156–6214. [CrossRef]

217. Narayanan, T.N.; Gupta, B.K.; Vithayathil, S.A.; Aburto, R.R.; Mani, S.A.; Taha-Tijerina, J.; Xie, B.; Kaipparettu, B.A.; Torti, S.V.; Ajayan, P.M. Hybrid 2d nanomaterials as dual-mode contrast agents in cellular imaging. *Adv. Mater.* **2012**, *24*, 2992–2998. [CrossRef]

218. Peng, J.; Gao, W.; Gupta, B.K.; Liu, Z.; Romero-Aburto, R.; Ge, L.; Song, L.; Alemany, L.B.; Zhan, X.; Gao, G.; et al. Graphene quantum dots derived from carbon fibers. *Nano Lett.* **2012**, *12*, 844–849. [CrossRef]

219. Chen, T.; Yu, H.; Yang, N.; Wang, M.; Ding, C.; Fu, J. Graphene quantum dot-capped mesoporous silica nanoparticles through an acid-cleavable acetal bond for intracellular drug delivery and imaging. *J. Mater. Chem. B* **2014**, *2*, 4979–4982. [CrossRef]

220. Hai, X.; Wang, Y.; Hao, X.; Chen, X.; Wang, J. Folic acid encapsulated graphene quantum dots for ratiometric ph sensing and specific multicolor imaging in living cells. *Sens. Actuators B Chem.* **2018**, *268*, 61–69. [CrossRef]

221. Lee, B.H.; McKinney, R.L.; Hasan, M.T.; Naumov, A.V. Graphene quantum dots as intracellular imaging-based temperature sensors. *Materials* **2021**, *14*, 616. [CrossRef]

222. Malek, A.; Aouad, K.; El Khoury, R.; Halabi-Tawil, M.; Choucair, J. Chronic mercury intoxication masquerading as systemic disease: A case report and review of the literature. *Eur. J. Case Rep. Intern. Med.* **2017**, *4*, 000632. [CrossRef]

223. Zhao, X.; Gao, J.; He, X.; Cong, L.; Zhao, H.; Li, X.; Tan, F. DNA-modified graphene quantum dots as a sensing platform for detection of hg2+ in living cells. *RSC Adv.* **2015**, *5*, 39587–39591. [CrossRef]

224. Liu, M.; Liu, T.; Li, Y.; Xu, H.; Zheng, B.; Wang, D.; Du, J.; Xiao, D. A fret chemsensor based on graphene quantum dots for detecting and intracellular imaging of hg2+. *Talanta* **2015**, *143*, 442–449. [CrossRef]

225. Zhu, A.; Ding, C.; Tian, Y. A two-photon ratiometric fluorescence probe for cupric ions in live cells and tissues. *Sci. Rep.* **2013**, *3*, 2933. [CrossRef]

226. Fang, B.-Y.; Li, C.; Song, Y.-Y.; Tan, F.; Cao, Y.-C.; Zhao, Y.-D. Nitrogen-doped graphene quantum dot for direct fluorescence detection of al3+ in aqueous media and living cells. *Biosens. Bioelectron.* **2018**, *100*, 41–48. [CrossRef]

227. Liu, R.; Zhao, J.; Huang, Z.; Zhang, L.; Zou, M.; Shi, B.; Zhao, S. Nitrogen and phosphorus co-doped graphene quantum dots as a nano-sensor for highly sensitive and selective imaging detection of nitrite in live cell. *Sens. Actuators B Chem.* **2017**, *240*, 604–612. [CrossRef]

228. Ma, L.; Sun, S.; Wang, Y.; Jiang, K.; Zhu, J.; Li, J.; Lin, H. A graphene quantum dot-based fluorescent nanoprobe for hypochlorite detection in water and in living cells. *Microchim. Acta* **2017**, *184*, 3833–3840. [CrossRef]

229. Zhao, W.; Li, Y.; Yang, S.; Chen, Y.; Zheng, J.; Liu, C.; Qing, Z.; Li, J.; Yang, R. Target-activated modulation of dual-color and two-photon fluorescence of graphene quantum dots for in vivo imaging of hydrogen peroxide. *Anal. Chem.* **2016**, *88*, 4833–4840. [CrossRef]

230. Wang, X.; Wang, Y.; He, H.; Chen, X.; Sun, X.; Sun, Y.; Zhou, G.; Xu, H.; Huang, F. Steering graphene quantum dots in living cells: Lighting up the nucleolus. *J. Mater. Chem. B* **2016**, *4*, 779–784. [CrossRef]

231. Yang, K.; Hou, L.; Li, Z.; Lin, T.; Tian, J.; Zhao, S. A mitochondria-targeted ratiometric fluorescent nanoprobe for imaging of peroxynitrite in living cells. *Talanta* **2021**, *231*, 122421. [CrossRef] [PubMed]

232. Zheng, X.T.; Than, A.; Ananthanaraya, A.; Kim, D.-H.; Chen, P. Graphene quantum dots as universal fluorophores and their use in revealing regulated trafficking of insulin receptors in adipocytes. *Acs Nano* **2013**, *7*, 6278–6286. [CrossRef] [PubMed]

233. Ananthanarayanan, A.; Wang, Y.; Routh, P.; Sk, M.A.; Than, A.; Lin, M.; Zhang, J.; Chen, J.; Sun, H.; Chen, P. Nitrogen and phosphorus co-doped graphene quantum dots: Synthesis from adenosine triphosphate, optical properties, and cellular imaging. *Nanoscale* **2015**, *7*, 8159–8165. [CrossRef] [PubMed]

234. Nurunnabi, M.; Khatun, Z.; Reeck, G.R.; Lee, D.Y.; Lee, Y.-k. Near infra-red photoluminescent graphene nanoparticles greatly expand their use in noninvasive biomedical imaging. *Chem. Commun.* **2013**, *49*, 5079–5081. [CrossRef] [PubMed]

235. Hasan, M.T.; Gonzalez-Rodriguez, R.; Lin, C.-W.; Campbell, E.; Vasireddy, S.; Tsedev, U.; Belcher, A.M.; Naumov, A.V. Rare-earth metal ions doped graphene quantum dots for near-ir in vitro/in vivo/ex vivo imaging applications. *Adv. Opt. Mater.* **2020**, *8*, 2000897. [CrossRef]

236. Zhang, M.; Bai, L.; Shang, W.; Xie, W.; Ma, H.; Fu, Y.; Fang, D.; Sun, H.; Fan, L.; Han, M.; et al. Facile synthesis of water-soluble, highly fluorescent graphene quantum dots as a robust biological label for stem cells. *J. Mater. Chem.* **2012**, *22*, 7461–7467. [CrossRef]

237. Ko, N.; Nafiujjaman, M.; Lee, J.; Lim, H.-N.; Lee, Y.-k.; Kwon, I. Graphene quantum dot-based theranostic agents for active targeting of breast cancer. *RSC Adv.* **2017**, *7*, 11420–11427. [CrossRef]

238. Nigam, P.; Waghmode, S.; Louis, M.; Wangnoo, S.; Chavan, P.; Sarkar, D. Graphene quantum dots conjugated albumin nanoparticles for targeted drug delivery and imaging of pancreatic cancer. *J. Mater. Chem. B* **2014**, *2*, 3190–3195. [CrossRef]

239. Wang, X.; Sun, X.; Lao, J.; He, H.; Cheng, T.; Wang, M.; Wang, S.; Huang, F. Multifunctional graphene quantum dots for simultaneous targeted cellular imaging and drug delivery. *Colloids Surf. B: Biointerfaces* **2014**, *122*, 638–644. [CrossRef]

240. Vahedi, N.; Tabandeh, F.; Mahmoudifard, M. Hyaluronic acid–graphene quantum dot nanocomposite: Potential target drug delivery and cancer cell imaging. *Biotechnol. Appl. Biochem.* **2021**. [CrossRef]

241. Zhao, Q.; Huang, C.; Li, F. Phosphorescent heavy-metal complexes for bioimaging. *Chem. Soc. Rev.* **2011**, *40*, 2508–2524. [CrossRef]

242. Suhling, K.; French, P.M.W.; Phillips, D. Time-resolved fluorescence microscopy. *Photochem. Photobiol. Sci.* **2005**, *4*, 13–22. [CrossRef]

243. Gillam, T.A.; Sweetman, M.J.; Bader, C.A.; Morrison, J.L.; Hayball, J.D.; Brooks, D.A.; Plush, S.E. Bright lights down under: Metal ion complexes turning the spotlight on metabolic processes at the cellular level. *Coord. Chem. Rev.* **2018**, *375*, 234–255. [CrossRef]

244. Lo, K.K.-W.; Zhang, K.Y. Iridium(iii) complexes as therapeutic and bioimaging reagents for cellular applications. *RSC Adv.* **2012**, *2*, 12069–12083. [CrossRef]

245. Coogan, M.P.; Fernández-Moreira, V. Progress with, and prospects for, metal complexes in cell imaging. *Chem. Commun.* **2014**, *50*, 384–399. [CrossRef]

246. Hostachy, S.; Policar, C.; Delsuc, N. Re(i) carbonyl complexes: Multimodal platforms for inorganic chemical biology. *Coord. Chem. Rev.* **2017**, *351*, 172–188. [CrossRef]

247. Amoroso, A.J.; Coogan, M.P.; Dunne, J.E.; Fernández-Moreira, V.; Hess, J.B.; Hayes, A.J.; Lloyd, D.; Millet, C.; Pope, S.J.A.; Williams, C. Rhenium fac tricarbonyl bisimine complexes: Biologically useful fluorochromes for cell imaging applications. *Chem. Commun.* **2007**, *29*, 3066–3068. [CrossRef]

248. Amoroso, A.J.; Arthur, R.J.; Coogan, M.P.; Court, J.B.; Fernández-Moreira, V.; Hayes, A.J.; Lloyd, D.; Millet, C.; Pope, S.J.A. 3-chloromethylpyridyl bipyridine fac-tricarbonyl rhenium: A thiol-reactive luminophore for fluorescence microscopy accumulates in mitochondria. *New J. Chem.* **2008**, *32*, 1097–1102. [CrossRef]

249. Bader, C.A.; Brooks, R.D.; Ng, Y.S.; Sorvina, A.; Werrett, M.V.; Wright, P.J.; Anwer, A.G.; Brooks, D.A.; Stagni, S.; Muzzioli, S.; et al. Modulation of the organelle specificity in re(i) tetrazolato complexes leads to labeling of lipid droplets. *RSC Adv.* **2014**, *4*, 16345–16351. [CrossRef]

250. Bader, C.A.; Shandala, T.; Carter, E.A.; Ivask, A.; Guinan, T.; Hickey, S.M.; Werrett, M.V.; Wright, P.J.; Simpson, P.V.; Stagni, S. A molecular probe for the detection of polar lipids in live cells. *PLoS ONE* **2016**, *11*, e0161557. [CrossRef]

251. Bader, C.A.; Sorvina, A.; Simpson, P.V.; Wright, P.J.; Stagni, S.; Plush, S.E.; Massi, M.; Brooks, D.A. Imaging nuclear, endoplasmic reticulum and plasma membrane events in real time. *FEBS Lett.* **2016**, *590*, 3051–3060. [CrossRef]

252. Caporale, C.; Bader, C.A.; Sorvina, A.; MaGee, K.D.M.; Skelton, B.W.; Gillam, T.A.; Wright, P.J.; Raiteri, P.; Stagni, S.; Morrison, J.L.; et al. Investigating intracellular localisation and cytotoxicity trends for neutral and cationic iridium tetrazolato complexes in live cells. *Chem.—A Eur. J.* **2017**, *23*, 15666–15679. [CrossRef]

253. Laha, P.; De, U.; Chandra, F.; Dehury, N.; Khullar, S.; Kim, H.S.; Patra, S. Alkyl chain-modified cyclometalated iridium complexes as tunable anticancer and imaging agents. *Dalton Trans.* **2018**, *47*, 15873–15881. [CrossRef]

254. Liu, J.-B.; Vellaisamy, K.; Li, G.; Yang, C.; Wong, S.-Y.; Leung, C.-H.; Pu, S.-Z.; Ma, D.-L. A long-lifetime iridium(iii) complex for lysosome tracking with high specificity and a large stokes shift. *J. Mater. Chem. B* **2018**, *6*, 3855–3858. [CrossRef]

255. Qiu, K.; Liu, Y.; Huang, H.; Liu, C.; Zhu, H.; Chen, Y.; Ji, L.; Chao, H. Biscyclometalated iridium(iii) complexes target mitochondria or lysosomes by regulating the lipophilicity of the main ligands. *Dalton Trans.* **2016**, *45*, 16144–16147. [CrossRef]

256. Qiu, K.; Huang, H.; Liu, B.; Liu, Y.; Huang, Z.; Chen, Y.; Ji, L.; Chao, H. Long-term lysosomes tracking with a water-soluble two-photon phosphorescent iridium(iii) complex. *ACS Appl. Mater. Interfaces* **2016**, *8*, 12702–12710. [CrossRef]

257. Li, J.; Chen, H.; Zeng, L.; Rees, T.W.; Xiong, K.; Chen, Y.; Ji, L.; Chao, H. Mitochondria-targeting cyclometalated iridium(iii) complexes for tumor hypoxic imaging and therapy. *Inorg. Chem. Front.* **2019**, *6*, 1003–1010. [CrossRef]

258. Zhang, C.; Liu, M.; Liu, S.; Yang, H.; Zhao, Q.; Liu, Z.; He, W. Phosphorescence lifetime imaging of labile zn2+ in mitochondria via a phosphorescent iridium(iii) complex. *Inorg. Chem.* **2018**, *57*, 10625–10632. [CrossRef]

259. Pasha, S.S.; Das, P.; Rath, N.P.; Bandyopadhyay, D.; Jana, N.R.; Laskar, I.R. Water soluble luminescent cyclometalated platinum(ii) complex—A suitable probe for bio-imaging applications. *Inorg. Chem. Commun.* **2016**, *67*, 107–111. [CrossRef]

260. Botchway, S.W.; Charnley, M.; Haycock, J.W.; Parker, A.W.; Rochester, D.L.; Weinstein, J.A.; Williams, J.A.G. Time-resolved and two-photon emission imaging microscopy of live cells with inert platinum complexes. *Proc. Natl. Acad. Sci. USA* **2008**, *105*, 16071. [CrossRef] [PubMed]

261. Yu, H.-j.; Zhao, W.; Xie, M.; Li, X.; Sun, M.; He, J.; Wang, L.; Yu, L. Real-time monitoring of self-aggregation of β-amyloid by a fluorescent probe based on ruthenium complex. *Anal. Chem.* **2020**, *92*, 2953–2960. [CrossRef] [PubMed]

262. Estalayo-Adrián, S.; Blasco, S.; Bright, S.A.; McManus, G.J.; Orellana, G.; Williams, D.C.; Kelly, J.M.; Gunnlaugsson, T. Water-soluble amphiphilic ruthenium(ii) polypyridyl complexes as potential light-activated therapeutic agents. *Chem. Commun.* **2020**, *56*, 9332–9335. [CrossRef] [PubMed]

263. Zhang, R.; Ye, Z.; Wang, G.; Zhang, W.; Yuan, J. Development of a ruthenium(ii) complex based luminescent probe for imaging nitric oxide production in living cells. *Chem.—A Eur. J.* **2010**, *16*, 6884–6891. [CrossRef] [PubMed]

264. Ji, S.; Guo, H.; Yuan, X.; Li, X.; Ding, H.; Gao, P.; Zhao, C.; Wu, W.; Wu, W.; Zhao, J. A highly selective off-on red-emitting phosphorescent thiol probe with large stokes shift and long luminescent lifetime. *Org. Lett.* **2010**, *12*, 2876–2879. [CrossRef]

265. Eliseeva, S.V.; Bünzli, J.-C.G. Lanthanide luminescence for functional materials and bio-sciences. *Chem. Soc. Rev.* **2010**, *39*, 189–227. [CrossRef]

266. Bunzli, J.-C.G.; Eliseeva, S.V. Intriguing aspects of lanthanide luminescence. *Chem. Sci.* **2013**, *4*, 1939–1949. [CrossRef]

267. Mathieu, E.; Sipos, A.; Demeyere, E.; Phipps, D.; Sakaveli, D.; Borbas, K.E. Lanthanide-based tools for the investigation of cellular environments. *Chem. Commun.* **2018**, *54*, 10021–10035. [CrossRef]

268. Mailhot, R.; Traviss-Pollard, T.; Pal, R.; Butler, S.J. Cationic europium complexes for visualizing fluctuations in mitochondrial atp levels in living cells. *Chemistry* **2018**, *24*, 10745–10755. [CrossRef]

269. Wu, J.; Che, W.; Liu, H.; Min, P.; Zheng, D. Development of a lysosome-targetable visible-light-excited europium(iii) complex-based luminescent probe to image hypochlorous acid in living cells. *Opt. Mater.* **2020**, *109*, 110273. [CrossRef]

270. Gillam, T.A.; Caporale, C.; Brooks, R.D.; Bader, C.A.; Sorvina, A.; Werrett, M.V.; Wright, P.J.; Morrison, J.L.; Massi, M.; Brooks, D.A.; et al. Neutral re(i) complex platform for live intracellular imaging. *Inorg. Chem.* **2021**, *60*, 10173–10185. [CrossRef]

271. Law, W.H.-T.; Lee, L.C.-C.; Louie, M.-W.; Liu, H.-W.; Ang, T.W.-H.; Lo, K.K.-W. Phosphorescent cellular probes and uptake indicators derived from cyclometalated iridium(iii) bipyridine complexes appended with a glucose or galactose entity. *Inorg. Chem.* **2013**, *52*, 13029–13041. [CrossRef]

272. Day, A.H.; Übler, M.H.; Best, H.L.; Lloyd-Evans, E.; Mart, R.J.; Fallis, I.A.; Allemann, R.K.; Al-Wattar, E.A.H.; Keymer, N.I.; Buurma, N.J.; et al. Targeted cell imaging properties of a deep red luminescent iridium(iii) complex conjugated with a c-myc signal peptide. *Chem. Sci.* **2020**, *11*, 1599–1606. [CrossRef]

273. Gill, M.R.; Garcia-Lara, J.; Foster, S.J.; Smythe, C.; Battaglia, G.; Thomas, J.A. A ruthenium(ii) polypyridyl complex for direct imaging of DNA structure in living cells. *Nat. Chem.* **2009**, *1*, 662–667. [CrossRef]

274. Lavis, L.D.; Raines, R.T. Bright ideas for chemical biology. *ACS Chem. Biol.* **2008**, *3*, 142–155. [CrossRef]

275. Wu, D.; Sedgwick, A.C.; Gunnlaugsson, T.; Akkaya, E.U.; Yoon, J.; James, T.D. Fluorescent chemosensors: The past, present and future. *Chem. Soc. Rev.* **2017**, *46*, 7105–7123. [CrossRef]

276. Miller, D.R.; Jarrett, J.W.; Hassan, A.M.; Dunn, A.K. Deep tissue imaging with multiphoton fluorescence microscopy. *Curr. Opin. Biomed. Eng.* **2017**, *4*, 32–39. [CrossRef]

277. Zheng, Q.; Juette, M.F.; Jockusch, S.; Wasserman, M.R.; Zhou, Z.; Altman, R.B.; Blanchard, S.C. Ultra-stable organic fluorophores for single-molecule research. *Chem. Soc. Rev.* **2014**, *43*, 1044–1056. [CrossRef]

278. Lei, Z.; Li, X.; Luo, X.; He, H.; Zheng, J.; Qian, X.; Yang, Y. Bright, stable, and biocompatible organic fluorophores absorbing/emitting in the deep near-infrared spectral region. *Angew. Chem. Int. Ed.* **2017**, *56*, 2979–2983. [CrossRef]

279. Hickey, S.M.; Ashton, T.D.; Boer, G.; Bader, C.A.; Thomas, M.; Elliott, A.G.; Schmuck, C.; Yu, H.Y.; Li, J.; Nation, R.L.; et al. Norbornane-based cationic antimicrobial peptidomimetics targeting the bacterial membrane. *Eur. J. Med. Chem.* **2018**, *160*, 9–22. [CrossRef]

280. Knorr, G.; Kozma, E.; Schaart, J.M.; Németh, K.; Török, G.; Kele, P. Bioorthogonally applicable fluorogenic cyanine-tetrazines for no-wash super-resolution imaging. *Bioconjugate Chem.* **2018**, *29*, 1312–1318. [CrossRef]

281. Jana, P.; Siva, A.; Soppina, V.; Kanvah, S. Live-cell imaging of lipid droplets using solvatochromic coumarin derivatives. *Org. Biomol. Chem.* **2020**, *18*, 5608–5616. [CrossRef]

282. Collot, M.; Kreder, R.; Tatarets, A.L.; Patsenker, L.D.; Mely, Y.; Klymchenko, A.S. Bright fluorogenic squaraines with tuned cell entry for selective imaging of plasma membrane vs. Endoplasmic reticulum. *Chem. Commun.* **2015**, *51*, 17136–17139. [CrossRef]

283. Chao, S.; Krejci, E.; Bernard, V.; Leroy, J.; Jean, L.; Renard, P.-Y. A selective and sensitive near-infrared fluorescent probe for acetylcholinesterase imaging. *Chem. Commun.* **2016**, *52*, 11599–11602. [CrossRef]

284. Holmila, R.J.; Vance, S.A.; Chen, X.; Wu, H.; Shukla, K.; Bharadwaj, M.S.; Mims, J.; Wary, Z.; Marrs, G.; Singh, R.; et al. Mitochondria-targeted probes for imaging protein sulfenylation. *Sci. Rep.* **2018**, *8*, 6635. [CrossRef]

285. Calatrava-Pérez, E.; Bright, S.A.; Achermann, S.; Moylan, C.; Senge, M.O.; Veale, E.B.; Williams, D.C.; Gunnlaugsson, T.; Scanlan, E.M. Glycosidase activated release of fluorescent 1,8-naphthalimide probes for tumor cell imaging from glycosylated 'pro-probes'. *Chem. Commun.* **2016**, *52*, 13086–13089. [CrossRef]

286. Ramu, V.; Kundu, P.; Kondaiah, P.; Chakravarty, A.R. Maloplatin-b, a cisplatin-based bodipy-tagged mito-specific "chemo-pdt" agent active in red light. *Inorg. Chem.* **2021**, *60*, 6410–6420. [CrossRef]

287. Shi, C.; Wu, J.B.; Pan, D. Review on near-infrared heptamethine cyanine dyes as theranostic agents for tumor imaging, targeting, and photodynamic therapy. *J. Biomed. Opt.* **2016**, *21*, 050901. [CrossRef]

288. Pham, T.C.; Nguyen, V.-N.; Choi, Y.; Lee, S.; Yoon, J. Recent strategies to develop innovative photosensitizers for enhanced photodynamic therapy. *Chem. Rev.* **2021**, *121*, 13454–13619. [CrossRef]